

# Synthesis, Structure and Physical Properties of “Wire-like” Metal Complexes

Masnun Naher,<sup>†</sup> Sören Bock,<sup>†</sup> Zakary M. Langtry, Kieran M. O’Malley, Alexandre N. Sobolev, Brian W. Skelton, Marcus Korb, and Paul J. Low\*



Cite This: <https://dx.doi.org/10.1021/acs.organomet.0c00685>



Read Online

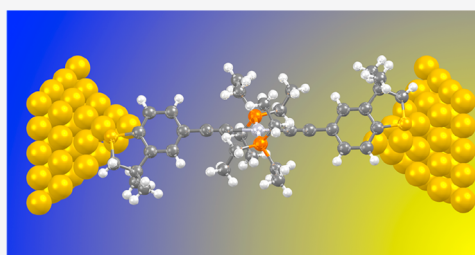
ACCESS |

Metrics & More

Article Recommendations

Supporting Information

**ABSTRACT:** The syntheses and crystallographically determined structures of metal complexes *trans*-[M(C≡CR)<sub>2</sub>L<sub>n</sub>] ( $ML_n = Ru(dppe)_2, Ru\{P(OEt)_3\}_4, Pt(PEt_3)_2$ ) featuring acetylide ligands further functionalized by aryl thioether groups are reported, together with those of analogous organic buta-1,3-diyne ( $RC \equiv CC \equiv CR$ ) and 1,4-diethynylbenzene ( $RC \equiv CC_6H_4C \equiv CR$ ) compounds for comparative purposes. The terminal thioether functional groups have an affinity for binding to the surface of gold electrodes and are considered as “anchor” groups in the design of molecules for study within metallmoleculemetal molecular junctions. The influence of the Lewis acidic and  $\pi$ -basic thioether moiety on a number of physical properties important to the electrical behavior of molecules within molecular junctions has been explored using spectroscopic, electrochemical, and quantum chemical methods. The thioether functional group serves as a moderately strong  $\pi$ -electron-donating substituent, similar in electronic character to the OMe group, resulting in relatively high lying HOMOs that are delocalized over the length of the molecule and well-suited to promote coherent tunneling within the junction. In addition, the facile oxidation processes and the relatively small reorganization energies associated with the one-electron oxidation of these compounds indicate the potential for effective hopping mechanisms of charge transport through longer structures based on these organometallic motifs.



## INTRODUCTION

The development of experiential platforms through which to construct electrode–molecule–electrode molecular junctions and measure molecular conductance (or resistance if one prefers) (Figure 1) has seen a renaissance in the field of molecular

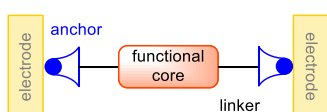


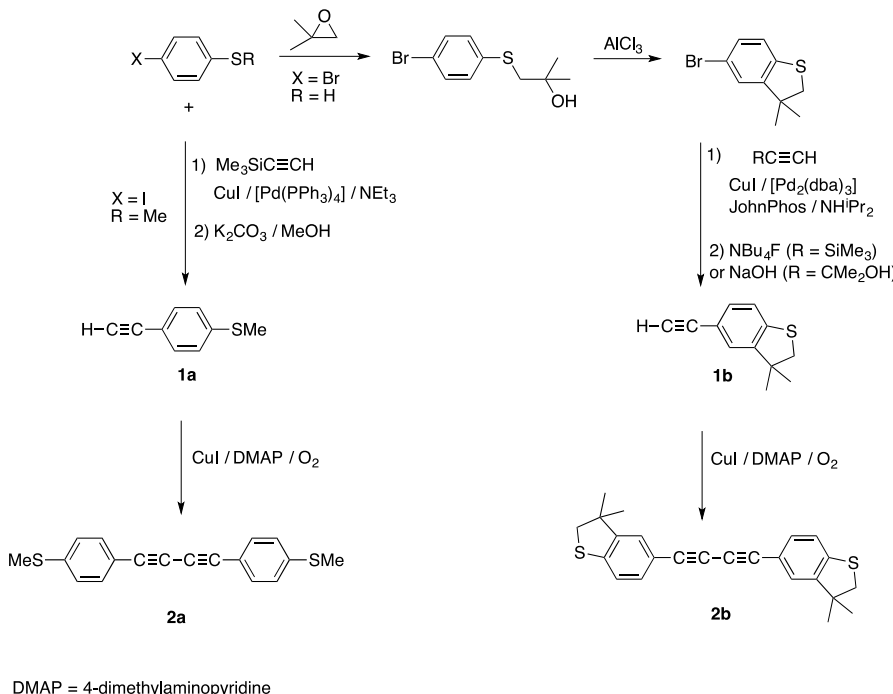
Figure 1. Cartoon depiction of an electrode–molecule–electrode molecular junction.

electronics.<sup>1–5</sup> This interest has in turn led to a demand for molecular structures in which some central moiety designed to offer some specified electronic function (e.g., wire-like conductance, bistable switching properties, rectification, transistor-like response, etc.) is connected, often via some intermediary “leads”, to “anchor groups”<sup>6</sup> suitable for contacting physically, electronically, and/or magnetically to the macroscopic electrodes of the junction (Figure 1).<sup>7,8</sup>

However, despite the appeal of such idealized “modular design” principles,<sup>9–13</sup> the electrical properties of the complete junction cannot be so simply partitioned. Beyond the elementary features of anchor groups, linkers, and the functional core required of molecules to be assembled within

molecular junctions, a more detailed design strategy requires consideration of the underlying mechanism of charge transport. For compounds in which the primary mechanism of conductance can be satisfactorily described in terms of coherent tunneling through a single rectangular barrier, important parameters include the length and height of the tunnel barrier. In turn, these concepts might be related to the distance between the designated atoms that provide electrode contacts in the anchor groups through the molecule,<sup>14</sup> and the energy offset between the electrode Fermi level and the molecular level (orbital) responsible for conductance,<sup>15</sup> respectively. As the molecular length increases, nonresonant hopping mechanisms in which the transporting charge progresses along the molecular backbone through one or more “steps” become increasingly important to the charge transport process.<sup>16</sup> The stepwise transfer of charge along the molecular backbone in the hopping mechanism implies that the transporting charge resides on the molecular backbone for a finite period of time. A description of the hopping

Received: October 20, 2020

**Scheme 1.** Preparation of Terminal Alkynes **1a,b** and Butadiynes **2a,b**

mechanism through a molecular junction therefore features concepts contained within Marcus theory and descriptions of charge transport in the junction can be made in terms of, for example, the Kusnetsev–Ulstrup two-step model, where the molecular reorganization energy accompanying a redox state change plays an important role in the overall process.<sup>17–19</sup> Destructive quantum interference can also play a profound role in the transmission of charge through a molecular backbone and is particularly important in cross-conjugated, branched, and pendant-decorated structures.<sup>20</sup>

As a result of these considerations, metal complexes have been identified as particularly interesting systems with which to construct molecular junctions.<sup>21–25</sup> Metal complexes and organometallic compounds are well suited to the modular design of molecules represented in Figure 1, with a well-defined geometry at the metal center and ready introduction of “linker” ligands further functionalized with anchor groups.<sup>26</sup> The nature of the metal and the ancillary ligands can be used to readily tune the frontier orbital energies,<sup>27</sup> while the additional magnetic, (opto)electronic, and redox properties of metal complexes provide ample scope for the introduction of useful properties within the junction.<sup>28–30</sup>

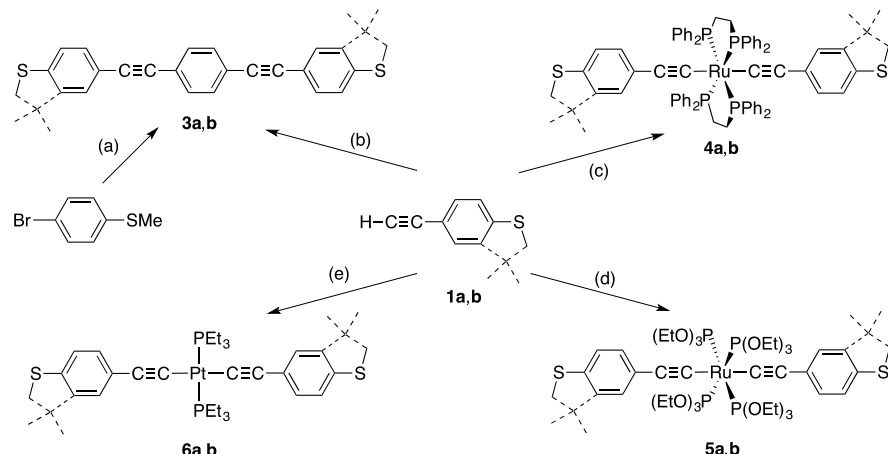
Here we report the syntheses and crystallographically determined structures of the metal complexes *trans*-[M(C≡CR)<sub>2</sub>L<sub>n</sub>] (ML<sub>n</sub> = Ru(dppe)<sub>2</sub>, Ru{P(OEt)<sub>3</sub>}<sub>4</sub>, Pt(PEt<sub>3</sub>)<sub>2</sub>), together with further investigations of the redox characteristics and electronic structures of the one-electron oxidation products, *trans*-[M(C≡CR)<sub>2</sub>L<sub>n</sub>]<sup>+</sup>, that would be important in future studies assessing coherent tunneling vs hopping-based mechanisms of charge transport<sup>19,31,32</sup> and redox-switching events within a molecular junction.<sup>18,33</sup> Data from closely related organic compounds are provided for comparison and completeness.

## RESULTS AND DISCUSSION

**Synthetic Chemistry.** The molecular design strategies for the compounds investigated here include functional groups intended to serve as contacts or anchors to secure the molecule within a molecular junction.<sup>8,34</sup> The acyclic thioether 4-thioanisole is a well-established anchor group capable of supporting both hole- and electron-mediated transport in molecular junctions.<sup>35</sup> Although not yet widely employed in studies of molecular junctions, the cyclic thioether benzodihydro[b]thiophene (BT) offers many desirable features for use as an anchor group, including high junction formation probability in STM-break junction experiments.<sup>36</sup> The BT anchor group has been used as an anchor group for the formation of molecular junctions from both organic compounds<sup>36–39</sup> and inorganic complexes<sup>40</sup> and supramolecular assemblies,<sup>41</sup> as have related six-membered cyclic thioethers.<sup>42</sup> Here we have chosen to use 3,3-dimethyl-2,3-dihydrobenzo[b]thiophene (DMBT) as a complementary anchor group,<sup>43</sup> with the 3,3-dimethyl groups being introduced to enhance the solubility of the resulting products as well as providing an element of synthetic expedience relative to the rather protracted synthesis of ethynyl BT derivatives.<sup>36</sup>

The parent alkyne 4-ethynylthioanisole (**1a**) is a well-known compound that is readily available from Sonogashira cross-coupling of commercially available 4-iodothioanisole with trimethylsilylacetylene ([Pd(PPh<sub>3</sub>)<sub>4</sub>]/CuI/NEt<sub>3</sub>) and subsequent removal of the protecting group (K<sub>2</sub>CO<sub>3</sub>/MeOH) (Scheme 1).

The related ethynyl-functionalized cyclic thioether 5-ethynyl-3,3-dimethyl-2,3-dihydrobenzo[b]thiophene (**2b**) was obtained from 5-bromo-3,3-dimethyl-2,3-dihydrobenzo[b]-thiophene, in turn prepared by a minor modification of the literature route.<sup>42</sup> The bromo moiety in 5-bromo-3,3-dimethyl-2,3-dihydrobenzo[b]thiophene is somewhat deactivated by the electron-donating cyclic thioether, prompting Bryce and colleagues to introduce a bromide/iodide exchange step in

Scheme 2. Preparation of Compounds and Complexes 3a,b–6a,b<sup>a</sup>

<sup>a</sup>Legend: (a) 0.5 equiv of 1,4-diethynylbenzene, [Pd(PPh<sub>3</sub>)<sub>4</sub>], CuI, NEt<sub>3</sub>; (b) 0.5 equiv of 1a,b, 1,4-dibromobenzene, [Pd<sub>2</sub>(dba)<sub>3</sub>], JohnPhos, CuI, NH'Pr<sub>2</sub>; (c) [RuCl(dppe)<sub>2</sub>]OTf, NaPF<sub>6</sub>, NEt<sub>3</sub>; (d) *trans*-[RuCl<sub>2</sub>{P(OEt)<sub>3</sub>}<sub>4</sub>], KPF<sub>6</sub>, NH'Pr<sub>2</sub>; (e) [PtCl<sub>2</sub>(PEt<sub>3</sub>)<sub>2</sub>], CuI, NEt<sub>3</sub>.

their synthesis of ethynyl derivatives of 2,3-dihydrobenzo[*b*]-thiophene.<sup>36</sup> After exploration of a range of palladium precursors and ligand systems, the [Pd<sub>2</sub>(dba)<sub>3</sub>]/JohnPhos/CuI catalyst system was found to be optimal to promote the smooth cross-coupling of 5-bromo-3,3-dimethyl-2,3-dihydrobenzo[*b*]thiophene with either trimethylsilylacetylene or 2-methyl-3-butyn-ol, thereby avoiding the halogen exchange step. Deprotection (NBu<sub>4</sub>F or NaOH/toluene respectively) gave 1b as a crystalline solid after workup (Scheme 1).

The terminal alkynes 1a and 1b smoothly homocoupled using the Navale catalyst system<sup>44,45</sup> to give the buta-1,3-diyne 2a (55%)<sup>46</sup> and 2b (56%), which offer a  $\pi$ -conjugated backbone of well-defined molecular length between the thioether anchor groups, making such compounds ideal for use in molecular electronics (Scheme 1).<sup>36,47</sup> However, derivatives of 1,4-bis(phenylethyynyl)benzene are perhaps the archetypal molecular wires and have formed the basis for many studies of the fundamental transport properties of molecular junctions,<sup>14,48–58</sup> meriting the preparation and characterization of such compounds for reference purposes. It proved convenient to prepare 3a (54%)<sup>59,60</sup> by the reaction of 1,4-diethynylbenzene with bromothioanisole under standard Sonogashira conditions while 3b (37%) was better obtained from 1,4-dibromobenzene and 1a (Scheme 2).

The metal complexes *trans*-[Ru(C≡CR)<sub>2</sub>(dppe)<sub>2</sub>] have proven to be effective test beds for the construction of molecular junctions based on organometallic complexes.<sup>27,28,61–68</sup> Here, reactions of [RuCl(dppe)<sub>2</sub>]OTf with 1a and 1b in the presence of NaPF<sub>6</sub> and triethylamine<sup>69–71</sup> gave 4a (98%) and 4b (65%), respectively (Scheme 2). With a view to decreasing potential adventitious contacts (short circuits) to the  $\pi$ -electron-rich aryl moieties of the dppe ligands within the junctions,<sup>72</sup> the closely related complexes *trans*-[Ru(C≡CR)<sub>2</sub>{P(OEt)<sub>3</sub>}<sub>4</sub>] bearing “insulating” trialkyl phosphite ancillary ligands were also prepared from reactions between *trans*-[RuCl<sub>2</sub>{P(OEt)<sub>3</sub>}<sub>4</sub>] and 1a or 1b in the presence of KPF<sub>6</sub> and diisopropylamine,<sup>73</sup> giving 5a (58%) and 5b (35%), respectively (Scheme 2). The behavior of square-planar platinum complexes *trans*-[Pt(C≡CR)<sub>2</sub>(PR'<sub>3</sub>)<sub>2</sub>] within molecular junctions has also attracted interest. Initially proposed as molecular insulators,<sup>74</sup> the wire-like properties of these systems have been gradually exposed.<sup>11,62,63,72,75,76</sup> The

platinum complexes 6a (38%)<sup>77</sup> and 6b (46%) were prepared by conventional CuI-catalyzed reactions of [PtCl<sub>2</sub>(PEt<sub>3</sub>)<sub>2</sub>] with 1a and 1b, respectively (Scheme 2).

**Molecular Structures.** The interpretation of conductance data from molecular junctions operating under a bias, often as a further function of electrode separation, is assisted by information concerning the molecular geometry within the junction and hence the molecular length. The crystallographically determined structures of the compounds 1a,<sup>78</sup> 2a,<sup>79</sup> and 3a<sup>80</sup> have been reported earlier by others, the structures of 1b–3b and 4a,b–6a,b being determined in the course of this work (Table 1). Plots of molecules of additional solvates (4a), disolvates (4b), and polymorphs (6b) and associated data are included in the Supporting Information.

The molecular structure of 1b (Figure 2) presents no unusual features, with an approximately linear acetylene moiety and expected parameters associated with the aromatic ring. The dihydrothiophene moiety adopts an envelope conformation, with C23 lying ca. 0.55 Å from the mean plane through S1–C1–C21–C22.

Compound 2b (Figure 3) adopts a linear structure in the solid state, with the two arene rings adopting a mutual angle of  $-19.134(2)^\circ$  and a clear pattern of long–short bond alternation along the buta-1,3-diyne backbone (Table 1). In the solid state, adjacent molecules are linked by a zigzag-like array following the *b* axis through intermolecular T-shaped C–H··· $\pi$  interactions involving H21B and the  $\pi$  system of the C13–C18 labeled aryl ring (Figure S1). There are no close S···S interactions.

In contrast to the solid-state structure of 3a, in which the aromatic rings adopt a largely coplanar orientation in the solid state,<sup>80</sup> the central phenylene ring of 3b, which sits on an inversion center, is canted by  $50.10(6)^\circ$  (root-mean-square deviation (rmsd) = 0.0009 Å) with respect to the outermost aryl rings, which are ideally coplanar ( $0.00(9)^\circ$ , rmsd = 0.0098 Å) (Figure 4). Weak T-shaped C–H··· $\pi$  interactions between C3 and C14 (3.3940(19) Å) dominate the crystal packing.

The complexes 4a (Figure S2) and 4b (Figure 5) both sit on centers of inversion, with the aryl rings of the anchor group lying approximately in the same plane and roughly intersecting the P1–Ru–P2A angles ( $\alpha = 97.78(2)^\circ$  (4a),  $97.95(2)^\circ$  (4b)) between both dppe fragments by  $\theta = 77, 71^\circ$  (4a) and  $\theta = 65,$

**Table 1.** Selected Crystallographically Determined Bond Lengths (Å) and Angles (deg) for Compounds **1a,b–3a,b** and Complexes **4a,b–6a,b** and Analogous Data from Optimized Geometries **1a,b–6a,b** and **[2a,b]<sup>+</sup>–[6a,b]<sup>+</sup>** Given in Italics

	M–C <sub>α</sub>	C <sub>α</sub> –C <sub>α</sub>	C <sub>α</sub> ≡C <sub>β</sub>	C <sub>β</sub> –C <sub>γ</sub>	C <sub>γ</sub> –S	S–C <sub>η</sub>	M–C <sub>α</sub> –C <sub>β</sub>	C <sub>α</sub> –C <sub>β</sub> –C <sub>γ</sub>	C <sub>γ</sub> –S–C <sub>η</sub>	d <sub>S,S</sub>	ref
<b>1a<sup>a</sup></b>	1.163(5)	1.433(5)	1.763(3)	1.797(3)	1.78.8(4)	103.2(2)					78
<b>1a</b>	1.204	1.43	1.838	1.878	179.99	103.35					
<b>1b<sup>a</sup></b>	1.24045(16)	1.4336(15)	1.7590(10)	1.8271(11)	178.06(11)	90.71(5)					
<b>1b</b>	1.204	1.43	1.833	1.906	179.93	89.02					
<b>2a<sup>b</sup></b>	1.207(2)	1.432(2)	1.7552(14)	1.7994(18)	178.88(16)	103.24(7)					79
<b>2a</b>	1.205(2)	1.432(2)	1.7567(14)	1.8016(18)	178.52(17)	103.3(8)					
<b>2a</b>	1.361	1.422	1.836	1.879	179.99	103.39					15.92
<b>2b</b>	1.212	1.422	1.836	1.879	179.99	103.39					
<b>2b</b>	1.322	1.226	1.391	1.798	1.880	179.97	104.37				15.76
<b>[2a]<sup>+</sup></b>	1.226	1.208(3)	1.431(3)	1.758(2)	1.822(2)	178.3(2)	90.91(9)				15.92
<b>[2b]<sup>+</sup></b>	1.361	1.207(3)	1.435(3)	1.759(2)	1.818(2)	178.4(2)	91.57(10)				15.66
<b>3a<sup>c</sup></b>	1.212	1.225	1.423	1.831	1.907	179.85	89.07				15.83
<b>3a</b>	1.333	1.225	1.392	1.792	1.909	179.63	90.20				15.68
<b>[3a]<sup>+</sup></b>	1.225	1.225	1.392	1.792	1.909	179.64	90.20				15.83
<b>3a</b>	1.203(5)	1.438(5)	1.769(4)	1.794(4)	179.8(4)	103.36(17)					
<b>3a</b>	1.204(5)	1.441(5)	1.766(3)	1.786(5)	178.2(4)	103.24(19)					
<b>3b<sup>c</sup></b>	1.424	1.209	1.425	1.837	1.879	179.94	103.38				20.23
<b>3b</b>	1.424	1.209	1.425	1.837	1.878	179.94	103.38				
<b>[3b]<sup>+</sup></b>	1.395	1.219	1.401	1.811	1.879	179.93	104.05				20.07
<b>3b</b>	1.395	1.219	1.401	1.811	1.879	179.93	104.05				
<b>3b</b>	1.4356(18)	1.2025(19)	1.4381(18)	1.7601(13)	1.8286(16)	176.91(14)	91.21(6)				19.99
<b>[3b]<sup>+</sup></b>	1.396	1.218	1.401	1.804	1.908	179.91	89.01				20.15
<b>4a<sup>c</sup></b>	2.073(3)	2.0604(18)	1.222(2)	1.432(2)	1.7691(18)	178.13(15)	104.05				
<b>4a</b>	2.094	1.228	1.428	1.781	1.815	177.66	103.85				18.72
<b>[4a]<sup>+</sup></b>	2.094	1.228	1.428	1.781	1.815	177.66	103.85				18.57
<b>4b<sup>c</sup></b>	2.043	1.232	1.420	1.771	1.815	177.77	104.10				
<b>4b</b>	2.095	1.228	1.420	1.771	1.815	177.77	104.10				
<b>4b<sup>c</sup>·CH<sub>2</sub>Cl<sub>2</sub></b>	2.063(3)	1.209(4)	1.444(4)	1.774(4) <sup>d</sup>	1.744(6) <sup>d</sup>	177.4(2)	92.11(3) <sup>e</sup>				18.49
<b>4b<sup>c</sup>·2CH<sub>2</sub>Cl<sub>2</sub></b>	2.0759(19)	1.213(3)	1.444(3)	1.762(2)	1.825(2)	175.03(17)	90.74(10)				18.57
<b>5a</b>	2.0623(15)	1.221(2)	1.433(2)	1.7700(17)	1.791(2)	178.82(13)	103.27(8)				
<b>5a</b>	2.096	1.226	1.429	1.777	1.839	177.49	103.87				18.72
<b>5a</b>	2.095	1.228	1.429	1.777	1.829	177.57	103.87				
<b>[4b]<sup>+</sup></b>	2.042	1.233	1.421	1.767	1.840	177.59	90.85				18.49
<b>5a</b>	2.0623(15)	1.219(2)	1.434(2)	1.7670(16)	1.791(2)	178.82(13)	103.27(8)				
<b>5a</b>	2.0663(15)	1.221(2)	1.433(2)	1.7700(17)	1.820(4)	177.39(13)	106.20(14)				
<b>5a</b>	2.096	1.226	1.429	1.781	1.815	178.30	103.87				

Table 1. continued

	M–C <sub>α</sub>	C <sub>α</sub> –C <sub>α</sub>	C <sub>α</sub> ≡C <sub>β</sub>	C <sub>β</sub> –C <sub>γ</sub>	C <sub>γ</sub> –S	S–C <sub>η</sub>	M–C <sub>α</sub> –C <sub>β</sub>	C <sub>α</sub> –C <sub>β</sub> –C <sub>γ</sub>	C <sub>γ</sub> –S–C <sub>η</sub>	d <sub>S,S</sub>	ref
[5a] <sup>+</sup>	2.093 2.019 2.055 2.061(5) 2.066(5)	1.225 1.238 1.23 1.213(7) 1.210(7)	1.428 1.409 1.421 1.421(7) 1.437(8)	1.781 1.764 1.772 1.761(7) 1.760(7)	1.815 1.815 1.815 1.949(11) 1.831(12)	179.40 178.99 178.75 176.4(4) 178.2(4)	179.92 179.78 179.63 175.4(7) 176.3(7)	103.87 104.29 104.05 88.4(5) 89.7(4)	18.54 18.30 18.30 18.30 18.30		
<b>5b</b>	2.095 2.094 2.094 2.015 2.062	1.225 1.225 1.225 1.239 1.228	1.429 1.429 1.429 1.407 1.422	1.777 1.777 1.777 1.757 1.769	1.839 1.839 1.839 1.840 1.840	178.01 178.01 179.60 178.65 179.14	179.02 90.48 90.50 179.25 179.82	90.48 90.48 90.50 91.21 90.79	18.64 18.64 18.64 18.46 18.46		
<b>6a</b>	1.9975(11) 2.027 2.028	1.2226(15) 1.225 1.225	1.4340(15) 1.432 1.432	1.7637(11) 1.785 1.785	1.7973(15) 1.820	179.37(10) 176.71	177.18(12) 176.71	102.96(6) 103.90	18.47 18.56		
<b>6a</b>	1.974 2.011	1.242 1.222	1.389 1.426	1.736 1.776	1.817 1.816	175.06 174.86	179.23 177.23	103.90 103.90	18.25		
<b>6b</b> (mol 1)	2.010(3) 1.999(3)	1.211(4) 1.213(4)	1.441(4) 1.441(4)	1.762(3) 1.760(3)	1.827(3) 1.830(3)	178.5(3) 179.4(4)	176.2(3) 179.4(4)	90.42(14) 90.70(14)			
<b>6b</b> (mol 2)	2.003(3)	1.212(4)	1.446(4)	1.756(3)	1.827(3)	177.3(3)	178.1(3)	90.78(14)	18.39		
<b>6b</b> (polymorph)	2.014(17)	1.21(3)	1.44(3)	1.772(17)	1.814(19)	177.3(16)	178(2)	90.4(8)			
<b>6b</b>	2.023 2.024	1.222 1.222	1.429 1.429	1.775 1.775	1.839 1.839	177.70 177.06	178.95 179.36	90.55 90.53			
<b>6b</b> <sup>+</sup>	1.992 2.027	1.247 1.227	1.395 1.436	1.733 1.783	1.848 1.849	177.04 177.83	179.09 178.90	92.36 90.59	18.40		

<sup>a</sup>CCDC reference number 234599. <sup>b</sup>CCDC reference number 950053. <sup>c</sup>CCDC reference number 1575159. <sup>d</sup>Disordered part: 1.975(16) Å. <sup>e</sup>Disordered part: 89.9(5)°.

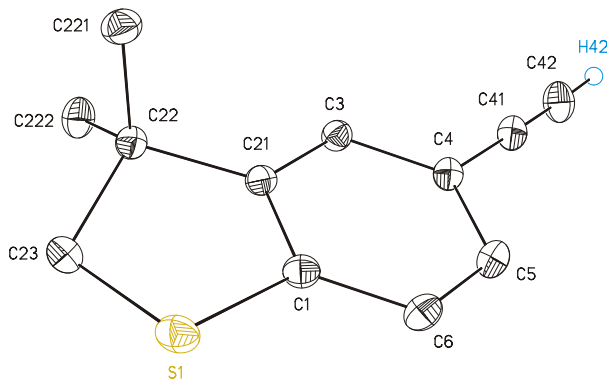


**Figure 2.** ORTEP drawing (50% probability level) of the molecular structure of **1b** with the atom-numbering scheme. All C-bonded hydrogen atoms except H42 have been omitted for clarity.

75° (**4b**), and therefore allowing a degree of  $d-\pi$  overlap with the molecular backbone.<sup>69</sup> There are no significant difference in bond lengths along the *trans*-bis(acetylide) backbone (Table 1), and the structures are entirely consistent with those of related complexes discussed elsewhere.<sup>69</sup>

The tetrakis(triethyl phosphite) complexes **5a** (Figure S5) and **5b** (Figure 6) offer the anticipated octahedral environment at ruthenium and *trans*-disposed acetylidy ligands.<sup>73</sup> The aromatic rings associated with the anchor groups are cantered with respect to each other by 55.67(2)° (**5a**) or 71.97(2)° (**5b**). The bond distances along the *trans*-bis(acetylide) backbone in **5a** and **5b** are strikingly consistent with each other and also with those of **4a** and **4b**, with no evidence for any significant influence of the ancillary ligands on the metal–alkynyl bonding (Table 1).

Complex **6a** (Figure S6) displays an almost ideal square-planar geometry at the platinum atom (P1–Pt1–C1, 89.90(3)°), which sits on an inversion center. The geometry at platinum in **6b** is somewhat more distorted in each of the two independent molecules in the asymmetric unit (Figure 7). The aromatic rings of the anchor groups are essentially coplanar and oriented orthogonally to the metal square plane. In the case of **6b**, strong S···S interactions link molecules into chain-like arrays in the solid state (Figure S8).

The data compiled in Table 1 indicate little systematic change in the structure of the arylacetylidy moieties as a function of the central moiety (2, bond; 3, phenylene ring; 4

and 5, ruthenium; 6, platinum), or the acyclic (**a**) or cyclic (**b**) nature of the thioether anchor. The constrained ring system in the cyclic thioether systems **b** results in only a very slight contraction of  $d_{S\cdots S}$  relative to the analogous acyclic thiomethyl derivatives **a** (Table 1). Together, the compounds and complexes **2a,b–6a,b** give a series of linear compounds with wire-like structures with S···S distances (“length”,  $d_{S\cdots S}$ ) ranging from 15.66 to 20.07 Å.

The exponential decay of conductance ( $G$ ) with distance in a simple single-barrier tunnel model of a molecular junction gives rise to the well-known expression

$$G \propto e^{-\beta l}$$

where  $l$  is the tunnel barrier length, usually approximated by the electrode separation in the junction and hence related to the molecular length, and  $\beta$  is a decay constant that reflects the wire-like efficacy of the molecule within the junction.<sup>14</sup> The similar  $d_{S\cdots S}$  values from the cyclic and thiomethyl functionalized pairs would permit a closer investigation of the nature of the anchor group largely free of complications arising from significant variations in molecular lengths. Similarly, the nearly identical values of  $d_{S\cdots S}$  for the ruthenium and platinum complexes **4–6** would also allow a comparison of the effects of the metal centers on the electrical characteristics of a junction largely free of the influence of variation in molecular lengths.

**Electrochemistry.** Estimates of the relative tunnel barrier heights or energy of a key transport channel (molecular orbital) relative to the electrode Fermi level have been made in studies conducted elsewhere from electrochemically determined oxidation potentials as a proxy for HOMO energy levels<sup>15</sup> and DFT calculations.<sup>9</sup> In addition, redox processes associated with a molecule within a junction can lead to in situ doping of the molecular species<sup>27</sup> or switching events as a function of the junction bias.<sup>28</sup> Further consideration of molecular conductance mediated by hole (electron) hopping mechanisms also raises interest in the electronic structures of the one-electron-oxidation (-reduction) products and associated reorganization energies. However, a note of caution is made, in that these approaches neglect the effect of the molecule–electrode interface and concepts such as charge pinning within the junction, the influence of solvation and ion-pairing on electrochemical potentials, and basis set and functional dependence of DFT estimates of orbital energies. Nevertheless, these concepts raise interest in the electro-

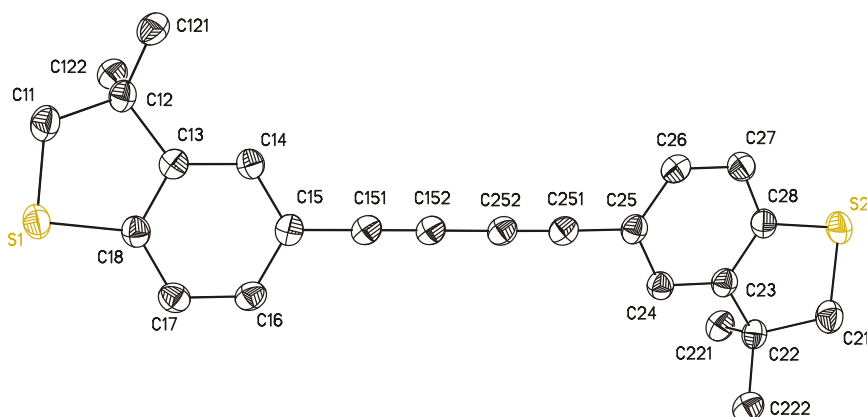


**Figure 3.** ORTEP drawing (50% probability level) of the molecular structure of **2b** with the atom-numbering scheme. All hydrogen atoms have been omitted for clarity.

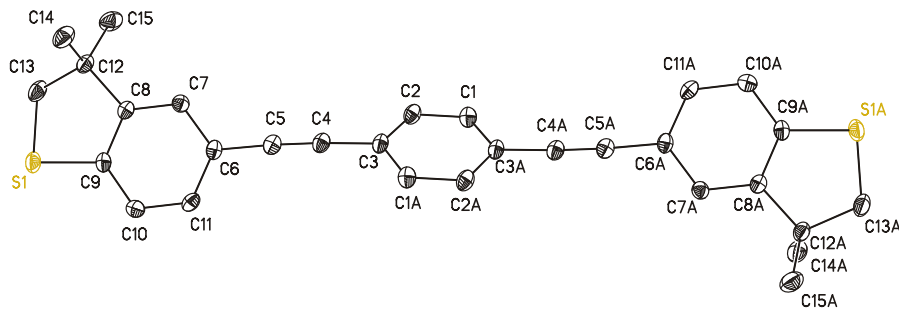


**Figure 4.** ORTEP drawing (50% probability level) of the molecular structure of **3b** with the atom-numbering scheme. All hydrogen atoms have been omitted for clarity. Symmetry operation for generating equivalent atoms: (A)  $-2 - x, 3 - y, 2 - z$ .

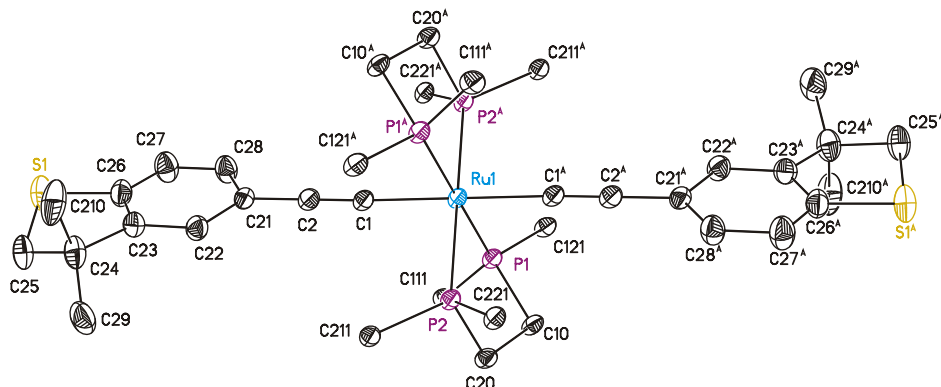


**Figure 5.** ORTEP drawing (50% probability level) of the molecular structure of **4b**- $\text{CH}_2\text{Cl}_2$  with the atom-numbering scheme. Hydrogen atoms, one disordered molecule of  $\text{CH}_2\text{Cl}_2$ , disordered parts of the DMBT moiety (0.696:0.304 occupancy ratio), and the phenyl rings, except for their ipso atoms, have been omitted for clarity. Symmetry operation for generating equivalent atoms: (A)  $1 - x, -y, -z$ .

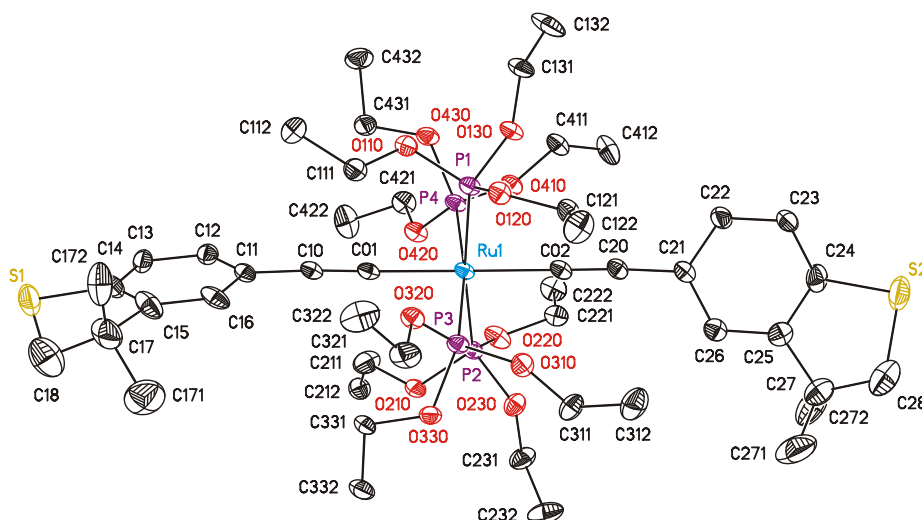


**Figure 6.** ORTEP drawing (50% probability level) of the molecular structure of **5b** with the atom-numbering scheme. All hydrogen atoms have been omitted for clarity.

chemical properties of the compounds and complexes **2a,b–6a,b** and the electronic structures of the resulting oxidation products.

At a platinum electrode, the organic buta-1,3-dynes **2a** and **2b** and 1,4-bis(aryleneethynyl)benzenes **3a** and **3b** each exhibited an irreversible oxidation process in their cyclic voltammograms (Table 2). The half-peak potentials ( $E_{\text{p}/2}$ )<sup>81</sup> indicate the more facile oxidation of compounds **3** vs compounds **2**, consistent with the extended  $\pi$  system of the 1,4-bis(aryleneethynyl)benzene core of **3** and indicative of a

higher-lying HOMO. The platinum complexes **6** also display an irreversible electrochemical response, with  $E_{\text{p}/2}$  values lower again than those of **3**. In contrast, the ruthenium complexes **4** and **5** displayed the near-reversible electrochemical response expected of species of this type<sup>69,73,82,83</sup> and, as would be expected, the oxidation potentials of complexes **4** and **5** are the lowest of the series explored here. The significant contribution from the alkynyl ligands to the oxidation processes of ruthenium acetylide complexes leads to a strong dependence of the oxidation potentials on the ligand substituents; here the

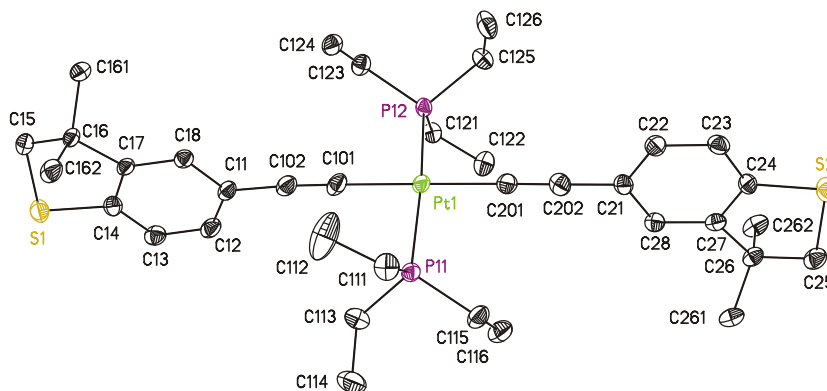


**Figure 7.** ORTEP drawing (50% probability level) of the molecular structure of one molecule of **6b** in the asymmetric unit with the atom-numbering schemes. All hydrogen atoms have been omitted for clarity.

**Table 2. Summary of Electrochemical Data from Compounds 2–6,<sup>a</sup> HOMO Energies Estimated from the Electrochemical Data ( $E_{\text{HOMO}}$ ), and Calculated HOMO Energies ( $E_{\text{HOMO}}'$ ), and Ionization Potentials (IP)**

compound	$E_{1/2}/\text{V}^{\text{b}}$	$ E_{\text{pa}} - E_{\text{pc}} /\text{mV}$	$i_{\text{pc}}/i_{\text{pa}}$	$E_{\text{HOMO}}/\text{eV}$	$E_{\text{HOMO}}'/\text{eV}$	$\text{IP}^{\text{c}}/\text{eV}$
2a	0.67 <sup>d</sup>		0	-5.5	-6.14	5.86
2b	0.87 <sup>d</sup>		0	-5.7	-6.07	5.79
3a	0.49 <sup>d</sup>		0	-5.3	-6.04	5.77
3b	0.50 <sup>d</sup>		0	-5.3	-5.99	5.72
4a	-0.10	60	1.0	-4.7	-4.97	4.47
4b	-0.12	60	0.9	-4.7	-4.95	4.45
5a	-0.06	80	1.0	-4.7	-5.12	4.76
5b	-0.13	60	0.9	-4.7	-5.09	4.74
6a	0.41 <sup>d</sup>		0	-5.2	-5.52	5.25
6b	0.37 <sup>d</sup>		0	-5.2	-5.45	5.18

<sup>a</sup>Conditions:  $\text{CH}_2\text{Cl}_2$  (0.1 M  $\text{NBu}_4\text{PF}_6$ ), Pt working electrode,  $\nu = 100 \text{ mV/s}$ . <sup>b</sup>Vs ferrocene/ferrocenium (i.e.,  $E(\text{Fc}/\text{Fc}^+) = 0.00 \text{ V}$ ) relative to an internal decamethylferrocene/decamethylferrocenium redox couple ( $E(\text{Fc}^*/\text{Fc}^{**}) = -0.53 \text{ V}$  vs Fc). <sup>c</sup>Calculated vertical ionization potential (vide infra). <sup>d</sup> $E_{p/2}$  of the anodic wave of an irreversible process.

thioether group has an effect similar to that of OMe on the redox potentials measured under the same conditions (*trans*-[Ru(C≡CC<sub>6</sub>H<sub>4</sub>OMe)<sub>2</sub>(dppe)<sub>2</sub>],  $E_{1/2} = -0.15 \text{ V}$ ; <sup>69</sup> *trans*-[Ru(C≡CC<sub>6</sub>H<sub>4</sub>OMe)<sub>2</sub>{P(OEt)<sub>3</sub>}<sub>4</sub>],  $E_{1/2} = -0.11 \text{ V}$ <sup>73</sup>). We note that the irreversible electrochemical response of the organic and platinum complexes is due to decomposition of the redox products at the electrode surface on the time scale of the electrochemical experiment. However, the residence time of charges on a long molecular wire (ca. 40 fs to  $0.1 \mu\text{s}$ )<sup>84</sup> during a hopping-based charge transport is very much less than the time taken for the potential sweep in the voltammetry experiments carried out here, and long molecular wires based on structures similar to **3** that conduct via hopping mechanisms are known.<sup>14,49</sup>

The HOMO levels of the compounds and complexes **2–6** can be broadly estimated from these electrochemical data relative to ferrocene ( $E_{\text{HOMO}} = 4.8 \text{ eV}$ ) (Table 2).<sup>85</sup> However, these estimates of orbital energies drawn from electrochemical data are convoluted by the effects of solvation, ion pairing, and reorganization energy on the electrochemical data and should be treated with appropriate caution and regarded as a relative measure rather than absolute values.

**Electronic Structure Calculations.** Electronic structure calculations (BLYP35/LANL2DZ for Ru, Pt/6-31G\*\* for all other atoms/CPCM CH<sub>2</sub>Cl<sub>2</sub> solvent model) were carried out for the complete suite of compounds **1a,b–6a,b** and the one-electron-oxidized products [2a,b]<sup>+</sup>–[6a,b]<sup>+</sup> most relevant to the hopping model of charge transport within a molecular

junctions. These calculations not only allow an estimate of the HOMO energy levels across the series but also provide some insight concerning the relative reorganization energies associated with the oxidation processes. We note that previous investigations have shown that the electronic structures of complexes *trans*-[Ru(C≡CC<sub>6</sub>H<sub>4</sub>R)<sub>2</sub>(dppe)<sub>2</sub>] are dependent on both the conformation and electronic character of the arylacetylidyne fragments.<sup>69</sup> Thus, while the major features of the electronic spectra of **4** and **5** can be attributed to transitions arising from the lowest energy conformer in which the arylacetylidyne ligands lie in the same plane and bisect a P–Ru–P angle, the fine details of the spectrum are more fully explained in terms of the population of a number of different conformers in solution that differ in the relative orientation of the arylacetylidyne fragments.<sup>69</sup> Given the fairly extensive exploration of these features in previous works, here attention will be directed to the most significant experimental features and the characteristics of the most stable (lowest energy) geometry.

Important bond lengths and angles from the geometry optimizations are given in Table 1 alongside the analogous parameters from the crystallographically determined structures. Plots, compositions, and energies of selected molecular orbitals of the neutral compounds and complexes **1a,b–6a,b** are given in Figures S9–S13, with the illustrative example of **5a** shown in Figure 8. These data provide a point for initial comparison of the electronic structures across the series. In each case, the HOMO is well described in terms of a  $\pi$ -electron system

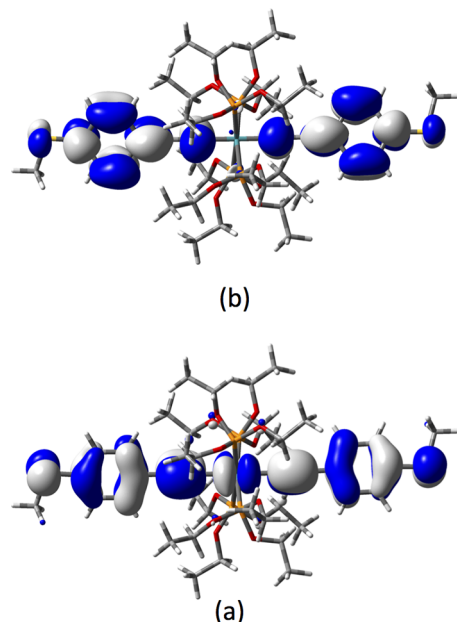


**Figure 8.** (a) HOMO and (b) LUMO of **5a** (surfaces plotted at  $\pm 0.02$  ( $e/\text{bohr}^3$ ) $^{1/2}$ ).

distributed along the length of the molecular backbone. The sulfur atoms of the anchor groups make a significant contribution to the HOMOs, as summarized in Table 3.

The HOMO energies ( $E_{\text{HOMO}}$ , Table 4) vary in the expected manner, increasing in energy with (idealized) conjugation length for **1–3** and higher again for the readily oxidized ruthenium complexes **4** ( $E_{1/2} = -0.13$  V vs ferrocene/ferrocenium) and **5** ( $E_{1/2} = -0.05$  V vs ferrocene/ferrocenium). The contributions from low-lying  $6s$ ,  $6p$ , and  $5d$  orbitals to the bonding in square-planar Pt complexes **6** decrease the HOMO energy, which is calculated to be lower lying than those of **4** and **5** but higher than those of the organic compounds (Table 4).

For the organic compounds **1–3** the LUMO is well described as the  $\pi^*$  orbital counterpart of the HOMO (Figure S9), decreasing in energy with increasing conjugation length and causing the expected decrease in the HOMO–LUMO gap from **1** to **2** to **3** (Table 4). This trend in orbital energies is consistent with the decreasing wavenumbers of the lowest energy optical transition in these compounds (Table 4 and Figures S18–S20), which in turn is reproduced by TD-DFT calculations (Table 4).

In the case of the dppe-coordinated complexes **4a** and **4b**, the low-lying aryl phosphine  $\pi^*$  orbitals comprise the LUMO, while the  $\pi^*$  complement of the HOMO, which is delocalized along the molecular backbone, is found as the [LUMO+3] (Figure S10). The lowest energy optical absorption band is found at  $28570\text{ cm}^{-1}$  (**4a**; Figure S21) or  $28730\text{ cm}^{-1}$  (**4b**; Figure S21) and assigned by TD-DFT calculations (Table 4) to offer predominantly MLCT character associated with charge transfer to the dppe ligands. The most intense low-energy transitions in the phosphite complexes **5a** and **5b** correspond

largely to the HOMO–LUMO transition with  $\pi-\pi^*$  character, with weak LMCT bands also found at lower energies (Table 1 and Figure S22).

The particular nature of the metal–ligand bonding in the square-planar complexes ensures that the LUMO of platinum complexes **6a** and **6b** is an unoccupied  $6p_z$  orbital, while the  $\pi^*$  complement of the HOMO is found as the [LUMO+1] (Figures S12 and S13). In the case of **6a** and **6b** the HOMO–LUMO transition, which has significant LMCT character, is calculated to have low oscillator strength. The [HOMO-1]–LUMO and HOMO–[LUMO+1] transitions have similar character and mix to give more intense absorption features of similar energy (Table 4) and together account for the appearance of the optical spectra of these complexes (Figure S23). However, the variation in the character of the lowest energy electronic transitions of any appreciable intensity points to a significant challenge in using the “optical gap” as a measure of the HOMO–LUMO gap across the series (Table 4).

The optimized structures of the radical cations reveal informative trends, similarities, and differences between the organic compounds and the various organometallic complexes concerning the underlying electronic structures. An inspection of the structures reveals that the organic compounds [**2a,b**]<sup>+</sup> and [**3a,b**]<sup>+</sup> offer more cumulated character than their neutral precursors, with slightly longer  $C\equiv C$  ( $\Delta_{C\equiv C} +0.01$  Å) and shorter  $C-C$  ( $\Delta_{C-C} -0.03$  Å) bonds (Table 1). This suggests that the unpaired electron (or hole) is distributed more or less evenly over the molecular backbone, which is consistent with the distribution of the  $\beta$ -LUMO in each case (Figure S14). The conformers of the metal complexes [**4a,b**]<sup>+</sup> examined here also offer a symmetrical structure with slightly increased cumulenoid character on oxidation being evident from the small changes in bond lengths relative to those of [**4a,b**] ( $\Delta_{Ru-C} -0.05$ ;  $\Delta_{C\equiv C} +0.005$ ;  $\Delta_{C-C} -0.008$  Å). These relatively small changes across the molecular backbone are again consistent with the distribution and composition of the  $\beta$ -LUMO (Figure S15).

The molecular structures calculated for the tetrakis(triethylphosphite)-supported ruthenium complexes [**5a,b**]<sup>+</sup> and platinum complexes [**6a,b**]<sup>+</sup> are more consistent with the effects of oxidation being localized on one of the alkynyl ligands. Further inspection of the distribution and composition of the  $\beta$ -HOMO and  $\beta$ -LUMO in each case confirms that one of the alkynyl ligands plays an important role in the redox activity of these complexes (Figures S16 and S17), which might be described as ligand-based mixed-valence systems. The ligand redox activity of *trans*-[Ru(C≡CR){P(OEt)<sub>3</sub>}<sub>4</sub>] has been proposed on the basis of model computational results reported earlier,<sup>73</sup> and localized conformers of ligand-based redox character have been reported for *trans*-[Pt{C≡CC<sub>6</sub>H<sub>4</sub>NAr<sub>2</sub>}(PR<sub>3</sub>)<sub>2</sub>]<sup>+</sup> complexes bearing redox-active triarylamino-functionalized alkynyl ligands.<sup>86,87</sup>

**Reorganization Energies.** While the tunnel barrier height and length are important parameters describing tunneling through a single rectangular barrier, the Marcus-type

**Table 3. Summary of S Atom Contributions (%) to the HOMO and LUMO of Compounds and Complexes 1a,b–6a,b**

	<b>1a</b>	<b>1b</b>	<b>2a</b>	<b>2b</b>	<b>3a</b>	<b>3b</b>	<b>4a</b>	<b>4b</b>	<b>5a</b>	<b>5b</b>	<b>6a</b>	<b>6b</b>
S (LUMO)	3	3	4	4	2	2	0	0	4	4	0	0
S (HOMO)	42	42	26	26	18	20	8	8	10	12	18	18

**Table 4. Summary of the Onset and Apparent Maximum of the Lowest Energy Transition in the UV–Vis Spectra of 1a,b–6a,b, DFT Calculated HOMO and LUMO Energies, TD DFT Calculated Transitions, and Assignment<sup>a</sup>**

	$\bar{\nu}_{\text{onset}}/\text{cm}^{-1}$	$\bar{\nu}_{\text{max}}/\text{cm}^{-1}$	$E_{\text{HOMO}}/\text{eV}$	$E_{\text{HOMO}}/\text{eV}$	$E_{\text{LUMO}}/\text{eV}$	$\Delta E_{\text{HOMO-LUMO}}/\text{eV}$	TD DFT/ $\text{cm}^{-1}$	oscillator strength ( $f$ )	assignment
<b>1a</b>				−6.54	−0.48	6.06	39202	0.6790	HOMO–LUMO (96%)
<b>1b</b>				−6.45	−0.46	5.99	38314	0.5173	HOMO–LUMO (92%)
<b>2a</b>	26310	27470	−5.5	−6.14	−1.34	4.80	29534	1.8006	HOMO–LUMO (92%)
<b>2b</b>	26110	27030	−5.7	−6.07	−1.31	4.76	29284	1.7120	HOMO–LUMO (92%)
<b>3a</b>	25910	27100	−5.3	−6.04	−1.47	4.57	28526	2.6685	HOMO–LUMO (94%)
<b>3b</b>	25125	26660	−5.3	−5.99	−1.45	4.54	28294	2.5804	HOMO–LUMO (94%)
<b>4a</b>	25310	28570	−4.7	−4.97	−0.30	4.67	32228	1.13179	HOMO–[LUMO+3] (68%)
<b>4b</b>	25440	28730	−4.7	−4.95	−0.30	4.65	32045	1.2266	HOMO–[LUMO+3] (56%) HOMO–[LUMO+2] (16%)
<b>5a</b>	26180	29410	−4.7	−5.12	+0.30	5.42	30203 31155 34083	0.0026 0.0022 1.9374	HOMO–[LUMO+4] (71%) [HOMO-2]–[LUMO+4] (46%) [HOMO-1]–[LUMO+4] (36%) HOMO–LUMO (80%)
<b>5b</b>	26110	28670	−4.7	−5.09	+0.30	5.39	30156 31110 33852	0.0025 0.0023 1.8305	HOMO–[LUMO+4] (70%) [HOMO-3]–[LUMO+4] (12%) [HOMO-2]–[LUMO+4] (49%) [HOMO-1]–[LUMO+4] (34%) HOMO–LUMO (78%) [HOMO-1]–[LUMO+1] (17%)
<b>6a</b>	26600	28570	−5.2	−5.52	−0.07	5.45	33200 35358 35916 36605	0.0492 1.0573 0.7266 0.6591	HOMO–LUMO (88%) [HOMO-1]–LUMO (66%) HOMO–[LUMO+1] (19%) HOMO–[LUMO+1] (48%) [HOMO-2]–LUMO (67%)
<b>6b</b>	26040	28490	−5.2	−5.45	−0.05	5.40	33027 35478 35595	0.1205 0.9948 0.8148	HOMO–LUMO (88%) HOMO–[LUMO+1] (34%) [HOMO-1]–LUMO (45%) [HOMO-1]–[LUMO+2] (11%) [HOMO]–[LUMO+1] (36%) [HOMO-1]–LUMO (41%) [HOMO-1]–[LUMO+2] (13%)

<sup>a</sup>Estimates of the HOMO energy ( $E_{\text{HOMO}}$ ) from electrochemical data are given for comparison.

reorganization energy is a primary factor influencing the description of charge hopping through a molecular junction. Reorganization energies associated with the oxidation of each species ( $\lambda_{(0,+1)}$ ) were calculated from the optimized geometries of the wire-like species 2a',b'–6a',b' in both the neutral and radical cation electronic configurations and the relationship

$$\lambda_{(0,+1)} = [E_{(0,+1)} - E_{(0,0)}] + [E_{(+1,0)} - E_{(+1,+1)}]$$

where  $E_{(x,y)}$  is the energy of the molecule in the optimized geometry  $x$  with electronic configuration  $y$  (i.e.,  $E_{(0,0)}$  is the energy of the neutral molecule in the neutral geometry, which is taken as the energy reference point in each case,  $E_{(0,+1)}$  is the energy of the neutral molecule in the cation geometry, etc.) (Table 5 and Figure 9).<sup>88</sup>

Perhaps unsurprisingly, the larger values of the reorganization energy are associated with 5a,b and 6a,b, which also give

**Table 5. Summary of Molecular Energies and Reorganization Energies Associated with the One-Electron Oxidation of 2a,b–6a,b**

	$E_{(0,0)}/\text{eV}$	$E_{(0,+1)}/\text{eV}$	$E_{(+1,+1)}/\text{eV}$	$E_{(+1,0)}/\text{eV}$	$\lambda_{(0,+1)}/\text{eV}$
2a	0.00	0.13	5.73	5.86	0.26
2b	0.00	0.14	5.66	5.79	0.27
3a	0.00	0.12	5.66	5.77	0.23
3b	0.00	0.12	5.61	5.72	0.23
4a	0.00	0.13	4.34	4.47	0.26
4b	0.00	0.13	4.32	4.46	0.26
5a	0.00	0.18	4.58	4.76	0.36
5b	0.00	0.18	4.56	4.76	0.37
6a	0.00	0.14	5.03	5.25	0.37
6b	0.00	0.23	5.08	5.18	0.34

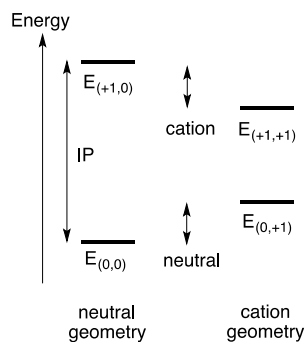


**Figure 9.** Sketch of the relative energies and geometries for the neutral and cation states of molecules  $[2a,b]^{n+}$ – $[6a,b]^{n+}$ . The energy of the neutral compound in the neutral geometry is taken as the reference point ( $E_{(0,0)} = 0 \text{ eV}$ ).

rise to the more localized one-electron-redox products. Nevertheless, the reorganization energies are generally quite low and are comparable to reorganization energies calculated from a number of triarylamine-based hole transport materials.<sup>89,90</sup> This suggests that compounds such as these might be suitable for the construction of longer wire-like molecules in which charge-hopping mechanisms would be expected to play a more significant role than coherent tunneling.

**Spectroelectrochemistry.** Spectroelectrochemical studies of metal acetylide and bis(acetylide) complexes have proven to be useful tools in the experimental investigation of the nature of redox processes and redox products<sup>91</sup> and were adopted here to gain supporting evidence for the computational results presented above. While the poor electrochemical reversibility of the electrochemical events associated with the organic buta-1,3-diyne **2a** and **2b** and 1,4-bis(aryleneethynyl)benzene compounds **3a** and **3b**, as well as the platinum complexes **6a** and **6b**, prohibited meaningful spectroelectrochemical investigations of these species and collection of data associated with  $[2]^+$ ,  $[3]^+$ , and  $[6]^+$ , the ruthenium species  $[4]^+$  and  $[5]^+$  were more readily studied. Although complexes of the general form *trans*- $[\text{Ru}(\text{C}\equiv\text{CR})_2(\text{dppe})_2]$  have been thoroughly investigated using spectroelectrochemical methods,<sup>69,83,92</sup> analogous studies of *trans*- $[\text{Ru}(\text{C}\equiv\text{CR})_2\{\text{P}(\text{OEt})_3\}_4]$  are far less common.

The IR spectroelectrochemical response of complexes **4a,b** and **5a,b** are illustrated in Figure 10. Each complex is characterized by a single  $\nu(\text{C}\equiv\text{C})$  band envelope in the narrow range  $2053$ – $2073 \text{ cm}^{-1}$ . In pairwise comparisons, the  $\nu(\text{C}\equiv\text{C})$  bands of the phosphine derivatives **4a** ( $2061 \text{ cm}^{-1}$ )

and **5a** ( $2073 \text{ cm}^{-1}$ ) fall at slightly larger wavenumbers in comparison to the comparable phosphite examples **4b** ( $2053 \text{ cm}^{-1}$ ) and **5b** ( $2067 \text{ cm}^{-1}$ ), consistent with a small additional back-bonding contribution from the more electron rich  $\text{Ru}\{\text{P}(\text{OEt})_3\}_4$  fragments to the alkynyl ligand moieties. Upon one-electron oxidation to the monocations in the spectroelectrochemical cell, the  $\nu(\text{C}\equiv\text{C})$  bands shift to one major, lower frequency band envelope by between  $170$  and  $165 \text{ cm}^{-1}$  (**4a**, **4b**) and between  $185$  and  $180 \text{ cm}^{-1}$  (**5a**, **5b**). The large shift to lower wavenumbers is indicative of a substantial role of the alkynyl ligands in the oxidation process, while the single principal feature in the  $\nu(\text{C}\equiv\text{C})$  spectra of the oxidized complexes indicates a predominant description of these species in terms of a delocalized electronic structure along the  $-\text{C}\equiv\text{C}-\text{Ru}-\text{C}\equiv\text{C}-$  chain. The breadth and asymmetry of the  $\nu(\text{C}\equiv\text{C})$  vibrational band envelopes in the oxidation products  $[\mathbf{4a,b}]^+$  and  $[\mathbf{5a,b}]^+$  is consistent with the presence of a number of conformers that differ in the relative orientation of the aromatic rings of the ethynyl ligands with respect to the  $\text{RuP}_4$  core in each case;<sup>69,73</sup> similar but less pronounced features are apparent in the neutral precursors. These different conformations will moderate the degree of  $d-\pi$  overlap along the molecular backbone. In the case of  $[\mathbf{5a}]^+$  and  $[\mathbf{5b}]^+$ , the presence of an additional weak feature at  $2022$  or  $2025 \text{ cm}^{-1}$ , respectively, is consistent with a population of conformers with more localized electronic structures  $\text{Ar}-\text{C}\equiv\text{C}-[\text{Ru}-\text{C}\equiv\text{C}-\text{Ar}]^+$ , consistent with the computational studies described above.

The similar electronic character of complexes *trans*- $[\text{Ru}(\text{C}\equiv\text{CR})_2(\text{dppe})_2]$  and *trans*- $[\text{Ru}(\text{C}\equiv\text{CR})_2\{\text{P}(\text{OEt})_3\}_4]$  is further evinced by the UV-vis-NIR spectra of **4a**, **4b**, **5a**, and **5b**, which are characterized in each case by a relatively high lying electronic transition near  $29000 \text{ cm}^{-1}$  (Figure 11). The monocations generated within the spectroelectrochemical cell exhibit a more complex series of electronic transitions with prominent features near  $35000$ ,  $23000$ , and  $7500 \text{ cm}^{-1}$ , together with a series of weaker transitions through the NIR region.

As noted above, the  $[\beta\text{-LUMO}]$  levels of  $[\mathbf{4a}]^+$  and  $[\mathbf{4b}]^+$  each have nodal properties and composition similar to those of the HOMO levels of the neutral precursors, consistent with the unpaired electron extensively delocalized over the molecular backbone. The low energy (NIR) absorption bands of the radical cations  $[\mathbf{4a}]^+$  and  $[\mathbf{4b}]^+$  are attributed by TD DFT calculations to the  $[\beta\text{-HOMO}]-[\beta\text{-LUMO}]$  transition with pronounced LMCT character with appreciable charge transfer from the S atoms as well as the ethynyl ligands to the metal center in each case.

The one-electron-oxidation products  $[\mathbf{5a}]^+$  and  $[\mathbf{5b}]^+$  give a more “localized” electronic structure, with the  $[\beta\text{-LUMO}]$  asymmetrically distributed over the ethynyl ligands, befitting a description of these compounds as ligand-based mixed-valence systems (Figure S16). The major NIR bands in these cases arising from the  $[\beta\text{-HOMO}]-[\beta\text{-LUMO}]$  transitions offer a degree of interligand charge-transfer character. Similar scenarios have been described for conformers of *trans*- $[\text{Ru}(\text{C}\equiv\text{CC}_6\text{H}_4\text{NH}_2)_2(\text{dppe})_2]^+$ .<sup>69</sup>

## CONCLUSIONS

A series of organic and organometallic complexes with “wire-like”  $\pi$ -conjugated backbone structures and acyclic or cyclic thioether “anchor groups” have been synthesized and characterized through crystallographic, electrochemical, spec-

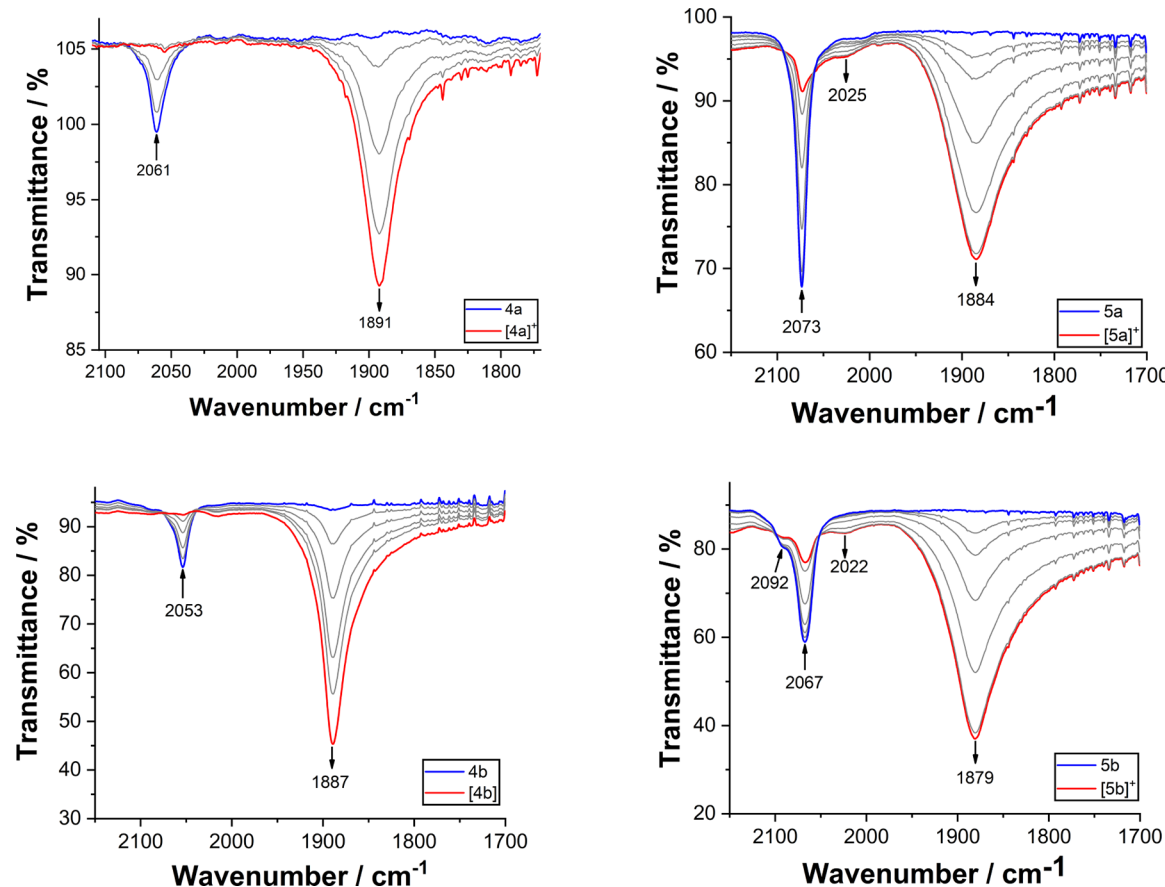


**Figure 10.** IR spectra of complexes  $[4a]^{n+}$ ,  $[4b]^{n+}$ ,  $[5a]^{n+}$ , and  $[5b]^{n+}$  ( $n = 0, 1$ ) recorded in a spectroelectrochemical cell ( $\text{CH}_2\text{Cl}_2/0.1 \text{ M} \text{ NBu}_4\text{PF}_6$ ).

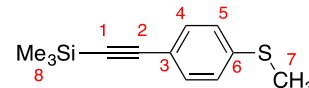
troelectrochemical, and computational methods. The molecular lengths, defined by the S···S distance ( $d_{\text{S}..\text{S}}$ ), are consistent across the ruthenium (**4a,b**; **5a,b**) and platinum (**6a,b**) metal complexes and are only slightly shorter than those in the 1,4-diethynylbenzene derivatives **3a,b**. The nature of the thioether has little bearing on the HOMO energy levels or redox potentials, which in turn are more sensitive to the nature of the central moiety (2, bond; 3, 1,4-phenylene; **4**, *trans*-Ru(dppe)<sub>2</sub>; **5**, *trans*-Ru{P(OEt)<sub>3</sub>}<sub>4</sub>; **6**, *trans*-Pt(PEt<sub>3</sub>)<sub>2</sub>). The delocalized nature of the electronic structures leads to only small changes in molecular structure and hence relatively low values of the Marcus-type reorganization energy on one-electron oxidation across the series. The localized electronic structures of  $[5a,b]^{+}$  and  $[6a,b]^{+}$  coupled with their low reorganization energy suggest that such motifs may be useful in the design of longer wire-like components that promote conductance via facile thermally activated charge-hopping mechanisms.

## ■ EXPERIMENTAL SECTION

**General Conditions: Synthetic Chemistry.** All reactions were performed under an  $\text{N}_2$  atmosphere using standard Schlenk techniques unless noted otherwise. Reaction solvents were purified and dried by appropriate means prior to distillation and storage under nitrogen. No special precautions were taken to exclude air or moisture during workup. The compounds **4**-ethynylthioanisole (**1a**),<sup>78,93</sup> *cis-/trans*-[PtCl<sub>2</sub>(PEt<sub>3</sub>)<sub>2</sub>],<sup>72</sup> *trans*-[RuCl<sub>2</sub>{P(OEt)<sub>3</sub>}<sub>4</sub>],<sup>94</sup> [RuCl(dppe)<sub>2</sub>]-OTf,<sup>95</sup> [Pd<sub>2</sub>(dba)<sub>3</sub>],<sup>96</sup> and [Pd(PPh<sub>3</sub>)<sub>4</sub>]<sup>97</sup> were prepared by literature methods or minor variations as described below. All other materials were obtained from commercial suppliers and used as received. NMR spectra were recorded in deuterated solvent solutions on Varian 300

MHz and Bruker Avance 500 and 600 MHz spectrometers and referenced against solvent resonances ( $\text{CHCl}_3$ , <sup>1</sup>H 7.26 ppm, <sup>13</sup>C{<sup>1</sup>H} 77.16 ppm;  $\text{CH}_2\text{Cl}_2$ , <sup>1</sup>H 5.32 ppm, <sup>13</sup>C{<sup>1</sup>H} 53.84 ppm;  $(\text{CH}_3)_2\text{CO}$ , <sup>1</sup>H 2.05 ppm, <sup>13</sup>C{<sup>1</sup>H} 29.84, 206.26 ppm). Infrared spectra were recorded on Thermo 6700 spectrometer from  $\text{CH}_2\text{Cl}_2$  solution in a cell fitted with  $\text{CaF}_2$  windows or an Agilent Technologies Cary 630 spectrometer using ATR sampling methods. High-resolution mass spectra were recorded using a Waters LCT Premier XE mass spectrometer using electrospray ionization or atmospheric pressure chemical ionization with leucine enkephalin as reference.

### Synthesis of 4-(Trimethylsilyl)ethynylthioanisole.<sup>98</sup>



To a solution of 4-iodothioanisole (1.00 g, 4.00 mmol) in dry, degassed triethylamine (25 mL), were added  $[\text{Pd}(\text{PPh}_3)_4]$  (46 mg, 0.04 mmol) and CuI (8 mg, 0.04 mmol). After addition of trimethylsilylacetylene (0.49 g, 5.00 mmol), the mixture was stirred for 4 h at room temperature. After this time, the solvent was removed in vacuo, the residue was extracted with hexanes, and the extracts were filtered through a silica plug. Removal of the solvent from the filtrate gave the product as a white, crystalline solid (0.88 g, 100%). IR (solid state, ATR)/cm<sup>-1</sup>:  $\nu(\text{C}\equiv\text{C})$  2153. <sup>1</sup>H NMR ( $\text{CDCl}_3$ , 500 MHz,  $\delta/\text{ppm}$ ): 0.24 (s, 9H, H<sup>8</sup>), 2.48 (s, 3H, H<sup>7</sup>), 7.15 (d,  $J = 8.1 \text{ Hz}$ , 2H, H<sup>5</sup>), 7.36 (d,  $J = 8.1 \text{ Hz}$ , 2H, H<sup>4</sup>). <sup>13</sup>C{<sup>1</sup>H} NMR ( $\text{CDCl}_3$ , 126 MHz,  $\delta/\text{ppm}$ ): 11.15 (C<sup>8</sup>), 15.45 (C<sup>7</sup>), 94.28 (C<sup>1</sup>), 105.01 (C<sup>2</sup>), 119.51 (C<sup>3</sup>), 125.78 (C<sup>5</sup>, C<sup>6</sup>), 132.36 (C<sup>3</sup>, C<sup>4</sup>), 139.73 (C<sup>6</sup>). MS (APCI-TOF)  $m/z$ : calcd for  $\text{C}_{12}\text{H}_{16}\text{OSSi}$  [ $\text{M}^+$ ] 220.0742; found 220.0734.

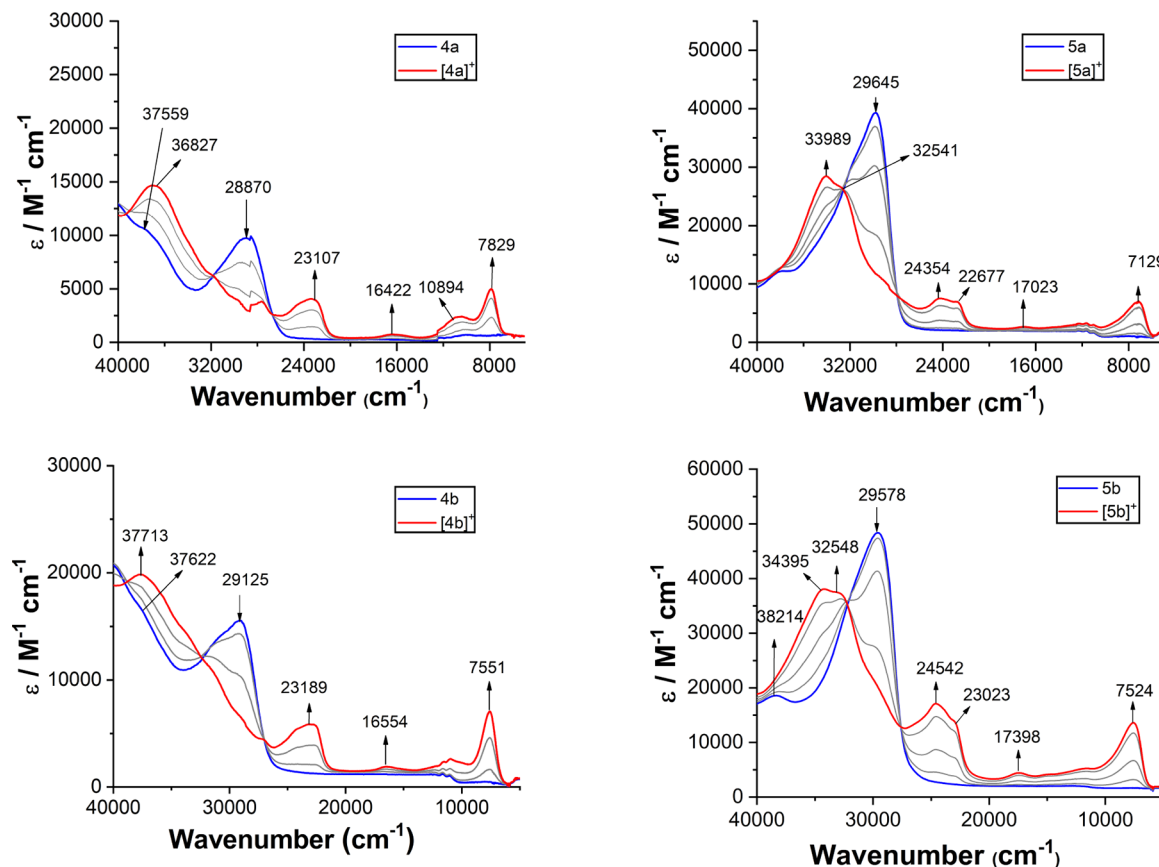
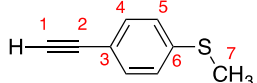


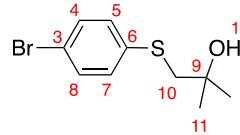
**Figure 11.** UV–vis–NIR spectra of complexes  $[4\text{a}]^{n+}$ ,  $[4\text{b}]^{n+}$ ,  $[5\text{a}]^{n+}$ , and  $[5\text{b}]^{n+}$  ( $n = 0, 1$ ) recorded in a spectroelectrochemical cell ( $\text{CH}_2\text{Cl}_2/0.1$  M  $\text{NBu}_4\text{PF}_6$ ).

*Synthesis of 4-Ethynylthioanisole (1a).*<sup>98</sup>



Potassium carbonate (0.83 g, 6 mmol) and 4-(trimethylsilylethynyl)-thioanisole (0.88 g, 4.00 mmol) were dissolved in methanol (50 mL) and stirred at room temperature for 2 h. After the solvent was removed under reduced pressure, the residue was purified by column chromatography (silica, hexane). After the solvent of the appropriate fraction was removed, the product was obtained as a dark yellow oil (0.54 g, 91%). IR ( $\text{CH}_2\text{Cl}_2/\text{cm}^{-1}$ ):  $\nu(\text{C}\equiv\text{C}-\text{H})$  3298,  $\nu(\text{C}\equiv\text{C})$  2108.  $^1\text{H}$  NMR ( $\text{CDCl}_3$ , 300 MHz,  $\delta/\text{ppm}$ ): 2.48 (s, 3H,  $\text{H}^7$ ), 3.07 (s, 1H,  $\text{H}^1$ ), 7.17 (d,  $J = 8.4$  Hz, 2H,  $\text{H}^5$ ), 7.40 (d,  $J = 8.4$  Hz, 2H,  $\text{H}^4$ ).  $^{13}\text{C}\{\text{H}\}$  NMR ( $\text{CDCl}_3$ , 126 MHz,  $\delta/\text{ppm}$ ): 15.36 ( $\text{C}^7$ ), 77.37 ( $\text{C}^1$ ), 83.55 ( $\text{C}^2$ ), 118.37 ( $\text{C}^3$ ), 125.81 ( $\text{C}^5$ ), 132.47 ( $\text{C}^3$ ), 140.16 ( $\text{C}^6$ ). MS (APCI-TOF)  $m/z$ : calcd for  $\text{C}_9\text{H}_8\text{S}$  [ $\text{M}]^+$  148.0347; found 148.0351.

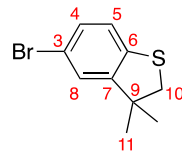
*Synthesis of 4-Bromophenylthio-2-methylpropan-2-ol.*<sup>42</sup>



A Schlenk flask was charged with acetone (150 mL), 4-bromothiophenol (3.00 g, 15.9 mmol), and 1,2-dimethyloxirane (2.28 g, 31.8 mmol) and the solution degassed by sparging with  $\text{N}_2$  for 20 min. To the degassed solution was added degassed triethylamine (10 mL), and the reaction mixture was stirred overnight at room temperature. The solvent was removed under reduced pressure to give the product as a colorless oil that solidified upon standing (4.00 g, 96%).  $^1\text{H}$  NMR ( $\text{CDCl}_3$ , 300 MHz,  $\delta/\text{ppm}$ ): 1.30 (s, 6H,  $\text{H}^{11}$ ), 2.09 (br s, 1H,  $\text{H}^{12}$ ), 3.09 (s, 2H,  $\text{H}^{10}$ ), 7.27 (d,  $J = 8.5$  Hz,  $\text{H}^5$ ), 7.39 (d,  $J = 8.5$  Hz,  $\text{H}^4$ ).  $^{13}\text{C}\{\text{H}\}$  NMR ( $\text{CDCl}_3$ , 500 MHz,

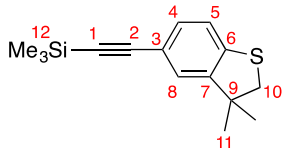
$\delta/\text{ppm}$ ): 28.81 (s,  $\text{C}^{11}$ ), 53.55 (s,  $\text{C}^{10}$ ), 70.85 (s,  $\text{C}^9$ ), 120.04 (s,  $\text{C}^3$ ), 130.98 (s,  $\text{C}^5,\text{C}^7$ ), 132.06 (s,  $\text{C}^4,\text{C}^8$ ), 136.48 (s,  $\text{C}^6$ ). MS (APCI-TOF)  $m/z$ : calcd for  $\text{C}_{10}\text{H}_{13}\text{BrOS}$  [ $\text{M}]^+$  261.9850; found 261.9870.

*Synthesis of 5-bromo-3,3-Dimethyl-2,3-dihydrobenzo[b]-thiophene.*<sup>42</sup>



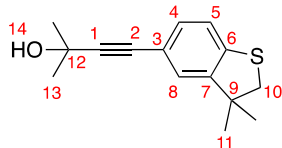
To a solution of 4-bromophenylthio-2-methyl-propan-2-ol (3.00 g, 11.5 mmol) in  $\text{CH}_2\text{Cl}_2$  (140 mL) was added aluminum trichloride (9.00 g, 67.5 mmol), causing the solution to quickly develop from colorless to dark red. The mixture was stirred for 7 days at room temperature. After this time, the mixture was filtered through a large silica plug (Caution! The evolution of HCl from unreacted  $\text{Al}_2\text{Cl}_6$  demands that this process be carried out in a well-ventilated hood.) and the plug washed with dichloromethane until the eluent was colorless (ca. 400 mL). Removing the solvent under reduced pressure yielded the crude product as a yellow oil (1.20 g, 44%). As this cyclization reaction was found to be capricious at larger scales, four separate preparations were typically carried out in parallel to give ca. 5 g of crude material, which was purified by Kugelrohr distillation (ca. 100 °C, ca. 1.5 mbar) to give ca. 4.2 g of the title compound as a yellow oil.  $^1\text{H}$  NMR ( $\text{CDCl}_3$ , 500 MHz,  $\delta/\text{ppm}$ ): 1.36 (s, 6H,  $\text{H}^{11}$ ), 3.09 (s, 2H,  $\text{H}^{10}$ ), 7.04 (d,  $J = 8$  Hz, 1H,  $\text{H}^5$ ), 7.14 (d,  $J = 2$  Hz, 1H,  $\text{H}^8$ ), 7.22 (dd,  $J = 8$  Hz, 2 Hz, 1H,  $\text{H}^4$ ).  $^{13}\text{C}\{\text{H}\}$  NMR ( $\text{CDCl}_3$ , 126 MHz,  $\delta/\text{ppm}$ ): 27.26 (s,  $\text{C}^{10}$ ), 47.50 (s,  $\text{C}^{11}$ ), 47.54 (s,  $\text{C}^9$ ), 117.81 (s,  $\text{C}^3$ ), 123.79 (s,  $\text{C}^5$ ), 126.06 (s,  $\text{C}^7$ ), 130.20 (s,  $\text{C}^4$ ), 139.77 (s,  $\text{C}^6$ ), 150.35 (s,  $\text{C}^8$ ). MS (APCI-TOF)  $m/z$ : calcd for  $\text{C}_{10}\text{H}_{11}\text{BrS}$  [ $\text{M}]^+$  243.9744; found 243.9745.

*Synthesis of 5-(Trimethylsilyl)ethynyl)-3,3-dimethyl-2,3-dihydrobenzo[b]thiophene.*



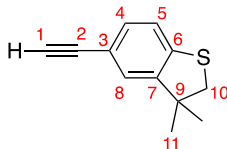
A Schlenk flask was charged with diisopropylamine (150 mL) and thoroughly degassed and fitted with an efficient condenser. To the solvent were added 5-bromo-3,3-dimethyl-2,3-dihydrobenzo[b]thiophene (3.40 g, 14.0 mmol), [Pd<sub>2</sub>(dba)<sub>3</sub>] (180 mg, 0.2 mmol), JohnPhos (120 mg, 0.4 mmol), CuI (76 mg, 0.4 mmol), and trimethylsilylacetylene (2.45 g, 25.0 mmol), and the mixture was stirred for 48 h at 50 °C. After the solvent was removed, the residue was purified by column chromatography on silica, from which the product was eluted with hexane. Removal of the solvent from the product-containing fractions gave the compound as a viscous oil (2.13 g, 59%). IR (solid state, ATR)/cm<sup>-1</sup>:  $\nu$ (C≡C) 2151. <sup>1</sup>H NMR (CDCl<sub>3</sub>, 500 MHz, δ/ppm): 0.19 (s, 9H, H<sup>12</sup>), 1.36 (s, 6H, H<sup>11</sup>), 3.09 (s, 2H, H<sup>10</sup>), 7.10 (d,  $J$  = 7.9 Hz, 1H, H<sup>5</sup>), 7.13 (d,  $J$  = 1.5 Hz, 1H, H<sup>8</sup>), 7.23 (dd,  $J$  = 7.9 Hz, 1.5 Hz, 1H, H<sup>4</sup>). <sup>13</sup>C{<sup>1</sup>H} NMR (CDCl<sub>3</sub>, 126 MHz, δ/ppm): 0.19 (s, C<sup>12</sup>), 27.44 (s, C<sup>10</sup>), 47.34 (s, C<sup>11</sup>), 47.40 (s, C<sup>9</sup>), 93.39 (s, C<sup>1</sup>), 105.64 (s, C<sup>2</sup>), 119.05 (s, C<sup>3</sup>), 122.26 (s, C<sup>5</sup>), 126.30 (s, C<sup>7</sup>), 131.37 (s, C<sup>4</sup>), 141.94 (s, C<sup>6</sup>), 148.18 (s, C<sup>8</sup>). MS (APCI-TOF) *m/z*: calcd for C<sub>12</sub>H<sub>12</sub>SSi [M]<sup>+</sup> 189.0693; found 189.0737.

*Synthesis of 4-(3,3-Dimethyl-2,3-dihydrobenzo[b]thiophen-5-yl)-2-methyl-3-butyne-2-ol.*



A solution of 5-bromo-3,3-dimethyl-2,3-dihydrobenzo[b]thiophene (3.14 g, 12.98 mmol) in dry NH<sub>3</sub>Pr<sub>2</sub> (50 mL) was thoroughly degassed and treated with 2-methylbut-3-en-2-ol (2.69 g, 27.5 mmol), (2-biphenylyl)-di-*tert*-butylphosphine (JohnPhos, 116 mg, 0.893 mmol), CuI (24 mg, 0.89 mmol), and [Pd<sub>2</sub>dba<sub>3</sub>] (0.057 g, 0.46 mmol). The reaction mixture was heated to 100 °C and allowed to react at this temperature overnight. After this time a second charge of catalyst and 2-methylbut-3-en-2-ol (1.0 mL) were added to the dark mixture and the reaction was allowed to proceed for a further day. After this time the reaction mixture was allowed to cool, the solvent removed under reduced pressure and the residue purified by column chromatography (silica, 1/1 CH<sub>2</sub>Cl<sub>2</sub>/hexane). The product was obtained as a yellow oil (2.46 g, 77%). IR (solid state, ATR)/cm<sup>-1</sup>:  $\nu$ (O-H) 3611–3100,  $\nu$ (C≡C) 2232. <sup>1</sup>H NMR (CDCl<sub>3</sub>, 500 MHz, δ/ppm): 1.36 (s, 6H, H<sup>10</sup>), 1.61 (s, 6H, H<sup>13</sup>), 1.98 (s, 1H, H<sup>14</sup>), 3.18 (s, 2H, H<sup>11</sup>), 7.10–7.08 (m, 2H, H<sup>4</sup> and H<sup>7</sup>), 7.17 (dd,  $J$  = 8.0 Hz, 2 Hz, 1H, H<sup>5</sup>). <sup>13</sup>C{<sup>1</sup>H} NMR (CDCl<sub>3</sub>, 126 MHz, δ/ppm): 27.46 (s, C<sup>10</sup>), 31.69 (s, C<sup>13</sup>), 47.36 (s, C<sup>11</sup>), 47.41 (s, C<sup>9</sup>), 65.83 (s, C<sup>12</sup>), 82.53 (s, C<sup>1</sup>), 93.19 (s, C<sup>2</sup>), 118.67 (s, C<sup>3</sup>), 122.32 (s, C<sup>5</sup>), 126.07 (s, C<sup>7</sup>), 130.98 (s, C<sup>4</sup>), 141.58 (s, C<sup>6</sup>), 148.28 (s, C<sup>8</sup>). MS (APCI-TOF) *m/z*: calcd for C<sub>15</sub>H<sub>18</sub>OS [M]<sup>+</sup> 246.1078; found 246.1054.

*Synthesis of 5-Ethynyl-3,3-dimethyl-2,3-dihydrobenzo[b]thiophene (1b).*

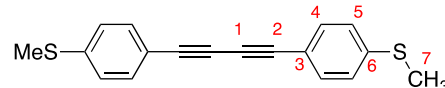


*Method 1.* A solution of 5-(trimethylsilyl)ethynyl)-3,3-dimethyl-2,3-dihydrobenzo[b]thiophene (2.13 g, 8.21 mmol) in THF (50 mL) was treated with NBu<sub>4</sub>F (commercial 1 M solution in THF (5% water), 8.3 mL) and the mixture stirred for 2 h. After the solvent was removed, the residue was extracted with hexanes (3 × 30 mL) and the combined extracts were washed with water (20 mL). The organic

phase was dried (MgSO<sub>4</sub>) and the volume reduced under reduced pressure before being filtered through a silica plug, with further elution with hexanes. After the solvent was removed from the combined fractions, the product was obtained as a yellow oil, which crystallized on standing (1.3 g, 84%). IR (CH<sub>2</sub>Cl<sub>2</sub>/cm<sup>-1</sup>):  $\nu$ (C≡C-H) 3296,  $\nu$ (C≡C) 2105. <sup>1</sup>H NMR (CDCl<sub>3</sub>, 500 MHz, δ/ppm): 1.37 (s, 6H, H<sup>11</sup>), 3.23 (s, 1H, H<sup>1</sup>), 3.59 (s, 2H, H<sup>10</sup>), 7.18 (dd,  $J$  = 7.9, 0.6 Hz, 1H, H<sup>5</sup>), 7.21–7.22 (m, 1H, H<sup>8</sup>), 7.25 (dd,  $J$  = 7.9, 1.5 Hz, 1H, H<sup>4</sup>). <sup>13</sup>C{<sup>1</sup>H} NMR (CDCl<sub>3</sub>, 126 MHz, δ/ppm): 27.3 (s, C<sup>11</sup>), 47.5 (s, C<sup>9</sup>), 47.9 (s, C<sup>10</sup>), 78.4 (s, C<sup>1</sup>), 84.5 (s, C<sup>2</sup>), 119.1 (s, C<sup>3</sup>), 123.0 (s, C<sup>5</sup>), 127.1 (s, C<sup>8</sup>), 132.0 (s, C<sup>4</sup>), 142.0 (s, C<sup>6</sup>), 148.4 (s, C<sup>7</sup>). MS (APCI) *m/z*: calcd for C<sub>12</sub>H<sub>12</sub>SSi [M + H]<sup>+</sup> 189.0693; found 189.0737.

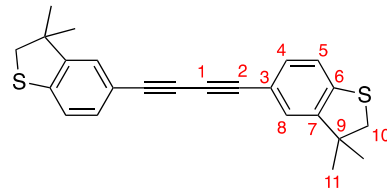
*Method 2.* A 100 mL Schlenk flask fitted with a distillation head was charged with 4-(3,3-dimethyl-2,3-dihydrobenzo[b]thienyl)-2-methyl-3-butyne-2-ol (2.46 g, 10.02 mmol) and dry toluene (50 mL). The distillation head was fitted to a short-path distillation apparatus and two-necked receiver flask. The receiver flask was vented to an oil bubbler through the second neck. The apparatus was purged with a steady flow of N<sub>2</sub> that swept through the assembly from the Schlenk flask to the oil bubbler. The reaction mixture was treated with freshly powdered NaOH (0.23 g, 5.7 mmol) and then heated to a gentle reflux point. The progress of the reaction could be followed by analytical TLC (hexane). After the reaction was judged to be complete (ca. 2 h) the reaction solution was filtered, and the solvent was removed under reduced pressure. The solid residue was purified by column chromatography (silica, hexanes) to give the title compound (0.94 g, 59%). Analytical data were as above.

*Synthesis of 2a.*<sup>46</sup>



A solution of 4-dimethylaminopyridine (16 mg, 0.130 mmol), 4-ethynylthioanisole (**1a**; 200 mg, 1.349 mmol), and CuI (13 mg, 0.068 mmol) in acetonitrile (15 mL) was stirred at room temperature in a vessel open to the atmosphere for 18 h. After the solvent was removed, the residue was washed with hexane three times to remove unreacted alkyne. The remaining product was further purified by passing through a silica plug to give a greenish yellow solid. Yield: 219 mg (55%). IR (solid state, ATR)/cm<sup>-1</sup>:  $\nu$ (C≡C) 2214, 2055. <sup>1</sup>H NMR (CDCl<sub>3</sub>, 300 MHz, δ/ppm): 2.49 (s, 6H, H<sup>7</sup>), 7.18 (d,  $J$ <sub>HH</sub> = 8 Hz, 4H, H<sup>4</sup>), 7.42 (d,  $J$ <sub>HH</sub> = 8 Hz, 4H, H<sup>5</sup>). <sup>13</sup>C{<sup>1</sup>H} NMR (CDCl<sub>3</sub>, 76 MHz, δ/ppm): 15.31 (C<sup>7</sup>), 74.23, 81.75 (C<sup>1</sup> and C<sup>2</sup>), 117.98 (C<sup>3</sup>), 125.79 (C<sup>5</sup>), 132.82 (C<sup>4</sup>), 140.98 (C<sup>6</sup>). MS (APCI-TOF) *m/z*: calcd for C<sub>18</sub>H<sub>14</sub>S<sub>2</sub> [M + H]<sup>+</sup> 295.0614; found 295.0615.

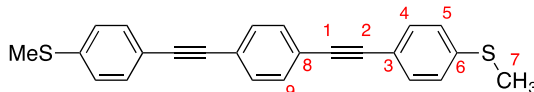
*Synthesis of 2b.*



A flask was charged with acetonitrile (15 mL), 4-dimethylaminopyridine (24 mg, 0.20 mmol), and CuI (19 mg, 0.10 mmol), and the mixture turned green after stirring for ca. 1 min. To this green solution was added 5-ethynyl-3,3-dimethyl-2,3-dihydrobenzo[b]thiophene (**1b**; 376 mg, 2.00 mmol), and the mixture was stirred in air for 18 h. After the solvent was removed, the residue was purified by column chromatography (hexane, silica). The crude product was then further purified by recrystallization from hot *n*-heptane (210 mg, 56%). Crystals suitable for X-ray single-crystal crystallography were obtained by recrystallization from hot *n*-heptane. IR (CH<sub>2</sub>Cl<sub>2</sub>/cm<sup>-1</sup>):  $\nu$ (C≡C) 2211, 2136. <sup>1</sup>H NMR (CDCl<sub>3</sub>, 500 MHz, δ/ppm): 1.37 (s, 12H, H<sup>11</sup>), 3.19 (s, 4H, H<sup>10</sup>), 7.13 (d,  $J$  = 8.0 Hz, 2H, H<sup>5</sup>), 7.18 (d,  $J$  = 1.5 Hz, 2H, H<sup>8</sup>), 7.28 (dd,  $J$  = 8.0, 1.5 Hz, H<sup>4</sup>). <sup>13</sup>C{<sup>1</sup>H} NMR (CDCl<sub>3</sub>, 126 MHz, δ/ppm): 27.5 (s, C<sup>11</sup>), 47.38 (s, C<sup>9</sup> or C<sup>10</sup>), 47.44 (s, C<sup>9</sup> or C<sup>10</sup>), 73.7 (s, C<sup>1</sup>), 82.2 (s, C<sup>2</sup>), 117.8 (s, C<sup>3</sup>), 122.5 (s, C<sup>5</sup>), 126.8 (s, C<sup>8</sup>), 131.8 (s, C<sup>4</sup>), 143.1 (s, C<sup>6</sup>), 148.5 (s, C<sup>7</sup>). HRMS

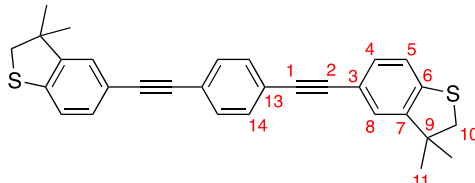
(APCI-TOF) *m/z*: calcd for  $C_{24}H_{23}S_2$  [M + H]<sup>+</sup> 375.1241; found 375.1231.

#### Synthesis of 3a.<sup>59</sup>



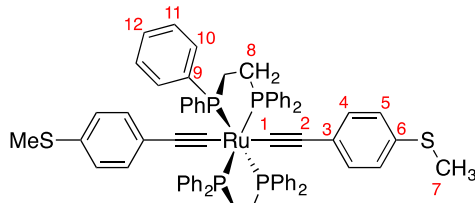
A solution of 1,4-diethynylbenzene (200 mg, 1.59 mmol) in dry, degassed triethylamine (20 mL) was treated with 4-bromothioanisole (676 mg, 3.33 mmol), [Pd(PPh<sub>3</sub>)<sub>4</sub>] (90 mg, 0.08 mmol), and CuI (15 mg, 0.08 mmol) and heated to the reflux point for 24 h. After this time, the solution was cooled, the solvent removed under reduced pressure, and the residue extracted into CH<sub>2</sub>Cl<sub>2</sub> before being washed with brine and subsequently aqueous 0.1 M KOH. The organic layer was dried (MgSO<sub>4</sub>) and the solvent removed to give the title compound as a yellow solid (318 mg, 54%). IR (solid state, ATR)/cm<sup>-1</sup>:  $\nu(C\equiv C)$  2116. <sup>1</sup>H NMR (CDCl<sub>3</sub>, 600 MHz,  $\delta$ /ppm): 2.51 (s, 6H, H<sup>7</sup>), 7.21 (d,  $J_{HH}$  = 8 Hz, 4H, H<sup>4</sup> or H<sup>5</sup>), 7.44 (d,  $J_{HH}$  = 8 Hz, 4H, H<sup>4</sup> or H<sup>5</sup>), 7.49 (s, 4H, H<sup>9</sup>). <sup>13</sup>C{<sup>1</sup>H} (CDCl<sub>3</sub>, 151 MHz,  $\delta$ /ppm): 15.50 (C<sup>7</sup>), 89.39, 91.24 (C<sup>1</sup> and C<sup>2</sup>), 119.43 (C<sup>3</sup>), 123.19 (C<sup>8</sup>), 126.00 (C<sup>5</sup>), 131.59, 132.03 (C<sup>4</sup> and C<sup>9</sup>), 139.79 (C<sup>6</sup>). MS (APCI-TOF) *m/z*: calcd for  $C_{24}H_{18}S_2$  [M]<sup>+</sup> 370.0851; found 370.0850.

#### Synthesis of 3b.



To a solution of 1,4-dibromobenzene (200 mg, 1.59 mmol) and 5-ethynyl-3,3-dimethyl-2,3-dihydrobenzo[b]thiophene (1b; 676 mg, 3.33 mmol) in diisopropylamine (15 mL) were added [Pd<sub>2</sub>(dba)<sub>3</sub>] (12 mg, 0.013 mmol), (2-biphenyl)-di-*tert*-butylphosphine- (JohnPhos, 4 mg, 0.013 mmol), and CuI (2.4 mg, 0.013 mmol). The reaction mixture was heated at reflux for 24 h, after which time the solvent was removed under reduced pressure and the residue purified by preparative TLC (1/9 CH<sub>2</sub>Cl<sub>2</sub>/hexane) to give the product as an orange solid (133 mg, 37%). The product could be further purified by recrystallization from hot n-heptane. Crystals suitable for X-ray diffraction were obtained by slow evaporation of a toluene solution. IR (CH<sub>2</sub>Cl<sub>2</sub>/cm<sup>-1</sup>):  $\nu(C\equiv C)$  2202. <sup>1</sup>H NMR (CDCl<sub>3</sub>, 600 MHz,  $\delta$ /ppm): 1.40 (s, 12H, H<sup>11</sup>), 3.21 (s, 4H, H<sup>10</sup>), 7.17 (d,  $J$  = 8.0 Hz, 2H, H<sup>5</sup>), 7.20 (d,  $J$  = 1.4 Hz, 2H, H<sup>8</sup>), 7.30 (dd,  $J$  = 8.0, 1.4 Hz, 2H, H<sup>4</sup>), 7.48 (s, 4H, H<sup>9</sup>). <sup>13</sup>C{<sup>1</sup>H} NMR (CDCl<sub>3</sub>, 126 MHz,  $\delta$ /ppm): 27.5 (s, C<sup>11</sup>), 47.4 (s, C<sup>9</sup>), 47.5 (s, C<sup>10</sup>), 88.8 (s, C<sup>2</sup>), 91.8 (s, C<sup>1</sup>), 119.0 (s, C<sup>3</sup>), 122.5 (s, C<sup>5</sup>), 123.2 (s, C<sup>13</sup>), 126.0 (s, C<sup>8</sup>), 131.0 (s, C<sup>4</sup>), 131.5 (s, C<sup>14</sup>), 142.0 (s, C<sup>6</sup>), 148.4 (s, C<sup>7</sup>). MS (APCI-TOF) *m/z*: 451 [M + H]<sup>+</sup>. HRMS (APCI-TOF) *m/z*: calcd for  $C_{30}H_{27}S_2$  [M + H]<sup>+</sup> 451.1554; found 451.1562. Anal. Calcd for  $C_{30}H_{26}S_2$ : C, 79.95; H, 5.82. Found: C, 79.87; H, 5.78.

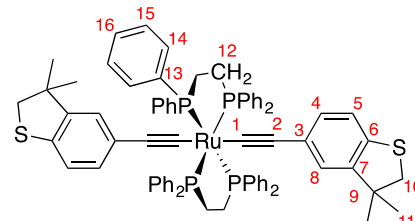
#### Synthesis of 4a.<sup>68</sup>



A solution of [RuCl(dppe)]OTf (0.100 g, 0.097 mmol), NaPF<sub>6</sub> (0.061 g, 0.36 mmol), and 4-ethynylthioanisole (1a; 0.039 g, 0.263 mmol) in CH<sub>2</sub>Cl<sub>2</sub> (5 mL) and triethylamine (1 mL) was stirred at room temperature for 1.5 h. During this time the initially red solution became yellow and large amounts of a pale precipitate formed, which was collected by filtration, washed with methanol, and air-dried to afford 4a as a yellow solid (0.110 g, 0.095 mmol, 98%). Crystals suitable for X-ray diffraction were obtained from CH<sub>2</sub>Cl<sub>2</sub>/MeOH by

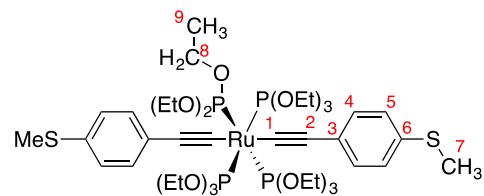
slow diffusion. IR (solid state, ATR)/cm<sup>-1</sup>:  $\nu(C\equiv C)$  2057. <sup>1</sup>H NMR (CDCl<sub>3</sub>, 600 MHz,  $\delta$ /ppm): 2.49 (s, 6H, H<sup>7</sup>), 2.57–2.63 (m, 8H, H<sup>8</sup>), 6.67 (d,  $J$  = 8.1 Hz, 4H, H<sup>3</sup>), 6.93–6.97 (m, 18H, H<sup>11</sup>), 7.06 (d,  $J$  = 8.1 Hz, 4H, H<sup>4</sup>), 7.14–7.19 (m, 8H, H<sup>12</sup>), 7.48–7.53 (m, 16H, H<sup>10</sup>). <sup>13</sup>C{<sup>1</sup>H} NMR (CDCl<sub>3</sub>, 151 MHz,  $\delta$ /ppm): 16.8 (s, C<sup>7</sup>), 31.60 (s, C<sup>8</sup>), 116.3 (m, C<sup>2</sup>), 126.8 (s, C<sup>5</sup>), 127.2 (s, C<sup>11</sup>), 128.1 (s, C<sup>3</sup>), 128.7 (s, C<sup>12</sup>), 130.6 (s, C<sup>4</sup>), 131.4 (s, C<sup>6</sup>), 134.4 (s, C<sup>10</sup>), 137.2 (m, C<sup>9</sup>) (C<sup>1</sup> not observed). <sup>31</sup>P{<sup>1</sup>H} NMR (CDCl<sub>3</sub>, 243 MHz,  $\delta$ /ppm): 53.8 (s). ESI(+)-MS *m/z*: calcd for  $C_{70}H_{62}P_4RuS_2$  1193.2320 [M + H]<sup>+</sup>; found 1193.2509 [M + H]<sup>+</sup>. Anal. Calcd for  $C_{70}H_{62}P_4RuS_2$ : C, 66.75; H, 5.05. Found: C, 67.57; H, 5.80.

#### Synthesis of 4b.



A solution of [RuCl(dppe)]OTf (100 mg, 0.092 mmol), NaPF<sub>6</sub> (31 mg, 0.19 mmol), and 5-ethynyl-3,3-dimethyl-2,3-dihydrobenzo[b]thiophene (1b; 37 mg, 0.20 mmol) in CH<sub>2</sub>Cl<sub>2</sub> (5 mL) and triethylamine (1 mL) was stirred at room temperature for 1.5 h. During this time the initially red solution changed to first orange and then yellow and large amounts of a pale precipitate formed. The precipitate was collected by filtration and washed with methanol to give the title compound as a pale yellow solid (76 mg, 65%). Crystals suitable for X-ray diffraction were obtained from CH<sub>2</sub>Cl<sub>2</sub>/EtOH. IR (solid state, ATR)/cm<sup>-1</sup>:  $\nu(C\equiv C)$  2051. <sup>1</sup>H NMR (CDCl<sub>3</sub>, 500 MHz,  $\delta$ /ppm): 1.38 (s, 12H, H<sup>11</sup>), 2.55–2.65 (m, 8H, H<sup>12</sup>), 3.17 (s, 4H, H<sup>10</sup>), 4.40 (d,  $J$  = 1.3 Hz, 2H, H<sup>8</sup>), 6.63 (dd,  $J$  = 8.0, 1.3 Hz, 2H, H<sup>4</sup>), 6.93–6.99 (m, 18H, H<sup>5</sup> and H<sup>15</sup>), 7.14–7.19 (m, 8H, H<sup>16</sup>), 7.51–7.56 (m, 16H, H<sup>14</sup>). <sup>13</sup>C{<sup>1</sup>H} NMR (CDCl<sub>3</sub>, 126 MHz,  $\delta$ /ppm): 27.6 (s, C<sup>11</sup>), 31.6 (m, C<sup>12</sup>), 47.3 (s, C<sup>9</sup>), 47.6 (s, C<sup>10</sup>), 116.7 (s, C<sup>2</sup>), 121.5 (s, C<sup>5</sup>), 124.7 (s, C<sup>8</sup>), 127.1 (br s, C<sup>3</sup> and C<sup>15</sup>), 128.7 (s, C<sup>16</sup>), 129.2 (s, C<sup>4</sup>), 133.9 (s, C<sup>6</sup>), 134.5 (s, C<sup>14</sup>), 137.3 (m, C<sup>13</sup>), 147.1 (s, C<sup>7</sup>) (a signal for C<sup>2</sup> could only be observed in the <sup>1</sup>H-<sup>13</sup>C-HMBC NMR spectrum, and no signal for C<sup>1</sup> could be observed at all). <sup>31</sup>P{<sup>1</sup>H} NMR (CDCl<sub>3</sub>, 202 MHz,  $\delta$ /ppm): 53.8 (s). ESI(+)-MS *m/z*: calcd for  $C_{76}H_{70}P_4RuS_2$  1272.2913 [M]<sup>+</sup>; found 1272.3032. Anal. Calcd for  $C_{76}H_{70}P_4RuS_2$ : C, 71.74; H, 5.54. Found: C, 71.58; H, 5.68.

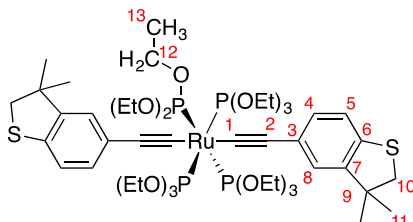
#### Synthesis of 5a.



A solution of [RuCl<sub>2</sub>{P(OEt)<sub>3</sub>}<sub>4</sub>] (0.108 g, 0.129 mmol), 4-ethynylanisole (1a; 0.100 g, 0.679 mmol) and KPF<sub>6</sub> (0.082 g, 0.446 mmol) in a mixture of ethanol (5 mL) and diisopropylamine (2.5 mL) was stirred at room temperature for 4 days under an inert atmosphere. The progress of the reaction was conveniently monitored by unlocked <sup>31</sup>P NMR spectroscopy, with the formation of the intermediate mono(alkynyl) complex *trans*-[RuCl(C≡CC<sub>6</sub>H<sub>4</sub>SMe)-{P(OEt)<sub>3</sub>}<sub>4</sub>] evinced by a singlet near 132.7 ppm, which was consumed over the course of the reaction and the bis(alkynyl) complex was formed ( $\delta_p$  ca. 137.7 ppm). Upon completion of the reaction, the solvent was removed from the reddish brown solution and the residue extracted with hexanes. The extracts were combined, filtered, and taken to dryness to give a reddish brown solid that was crystallized (CHCl<sub>3</sub>/MeOH) to give the title complex as yellow-brown crystals suitable for X-ray diffraction (80 mg, 58%). IR (solid state, ATR)/cm<sup>-1</sup>:  $\nu(C\equiv C)$  2104. <sup>1</sup>H NMR (CDCl<sub>3</sub>, 500 MHz,  $\delta$ /ppm): 1.19 (t,  $J$  = 7 Hz, 36H, H<sup>9</sup>), 2.43 (s, 6H, H<sup>7</sup>), 4.29 (q,  $J$  = 7 Hz,

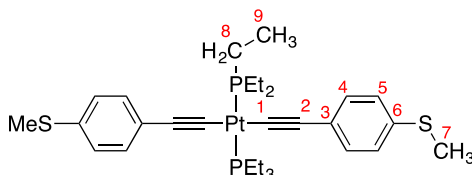
24H, H<sup>8</sup>), 6.94 (d,  $J$  = 8 Hz, 4H, H<sup>5</sup>), 7.04 (d,  $J$  = 8 Hz, 4H, H<sup>4</sup>). <sup>13</sup>C{<sup>1</sup>H} NMR ( $\text{CDCl}_3$ , 126 MHz,  $\delta$ /ppm): 16.52 (s, C<sup>7</sup>), 16.92 (s, C<sup>9</sup>), 60.95 (s, C<sup>8</sup>), 113.31 (s, C<sup>2</sup>), 127.28 (s, C<sup>3</sup>), 128.82 (s, C<sup>5</sup>), 130.44 (s, C<sup>4</sup>), 130.79 (s, C<sup>6</sup>) (C<sup>1</sup> not observed). <sup>31</sup>P{<sup>1</sup>H} NMR ( $\text{CDCl}_3$ , 202 MHz,  $\delta$ /ppm): 136.84 (s). ESI(+)-MS  $m/z$ : Calcd for  $\text{C}_{42}\text{H}_{75}\text{O}_{12}\text{P}_4\text{RuS}_2$  1061.2694 [M + H]<sup>+</sup>; found 1061.2766 [M]<sup>+</sup>, 1061.2694. Anal. Calcd for  $\text{C}_{42}\text{H}_{74}\text{O}_{12}\text{P}_4\text{RuS}_2$ : C, 47.58; H, 7.04. Found: C, 47.46; H, 6.97.

### Synthesis of 5b.



A solution of  $[\text{RuCl}_2(\text{P}(\text{OEt})_3)_4]$  (105 mg, 0.126 mmol) was dissolved in a dry, degassed solvent mixture of EtOH (5 mL) and diisopropylamine (2.5 mL). To the solution were added KPF<sub>6</sub> (95 mg, 0.51 mmol) and 5-ethynyl-3,3-dimethyl-2,3-dihydrobenzo[b]-thiophene (**1b**; 135 mg, 0.720 mmol). The solution was stirred for 7 days at room temperature. The progress of the reaction could be followed by unlocked <sup>31</sup>P NMR, showing the initial increase in the intensity of a peak near 132.7 ppm for the intermediate mono(alkynyl) complex, which was consumed over time with the formation of the bis(alkynyl) product ( $\delta_{\text{P}}$  ca. 137.8 ppm). When the reaction was judged to be complete, the solvent was removed from the reddish brown solution under reduced pressure and the residue extracted into hexanes. The combined extracts were filtered, and the solvent was removed to give a reddish brown solid that was crystallized ( $\text{CH}_2\text{Cl}_2/\text{MeOH}$ ) to give yellow-brown crystals of the title complex suitable for X-ray diffraction (47 mg, 35%). On occasion, the presence of an unidentified yellow impurity necessitated repeated crystallization to obtain analytically pure samples. IR (solid state, ATR)/cm<sup>-1</sup>:  $\nu(\text{C=C})$  2070. <sup>1</sup>H NMR ( $\text{CDCl}_3$ , 500 MHz,  $\delta$ /ppm): 1.21 (t,  $J$  = 7 Hz, 36H, H<sup>13</sup>), 1.31 (s, 12H, H<sup>11</sup>), 3.13 (s, 4H, H<sup>10</sup>), 4.31 (q,  $J$  = 7 Hz, 24H, H<sup>12</sup>), 6.77–6.80 (m, 4H, H<sup>4</sup> and H<sup>8</sup>), 6.93 (d,  $J$  = 8 Hz, 2H, H<sup>5</sup>). <sup>13</sup>C{<sup>1</sup>H} NMR ( $\text{CDCl}_3$ , 126 MHz,  $\delta$ /ppm): 16.6 (s, C<sup>13</sup>), 27.5 (s, C<sup>11</sup>), 47.1 (s, C<sup>9</sup>), 47.4 (s, C<sup>10</sup>), 61.0 (s, C<sup>12</sup>), 113.5 (s, C<sup>2</sup>), 115.0 (m, C<sup>1</sup>), 121.7 (s, C<sup>5</sup>), 124.9 (s, C<sup>8</sup>), 127.9 (s, C<sup>3</sup>), 128.8 (s, C<sup>4</sup>), 133.3 (s, C<sup>6</sup>), 147.3 (s, C<sup>7</sup>). <sup>31</sup>P{<sup>1</sup>H} NMR ( $\text{CDCl}_3$ , 202 MHz,  $\delta$ /ppm): 136.9 (s). HRMS (APCI-TOF)  $m/z$ : calcd for  $\text{C}_{48}\text{H}_{83}\text{O}_{12}\text{P}_4\text{RuS}_2$  [M + H]<sup>+</sup> 1141.3333; found 1141.3013. Anal. Calcd for  $\text{C}_{48}\text{H}_{82}\text{O}_{12}\text{P}_4\text{RuS}_2$ : C, 50.56; H, 7.25. Found: C, 50.45; H, 7.07.

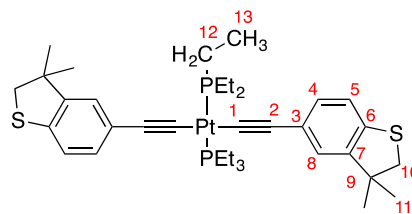
### Synthesis of 6a.



A Schlenk flask was charged with  $[\text{PtCl}_2(\text{PEt}_3)_2]$  (250 mg, 0.50 mmol), 4-ethynylthioanisole (**1a**, 220 mg, 1.49 mmol), CuI (2 mg, 0.01 mmol) and dry triethylamine (30 mL). The mixture was heated under reflux overnight. After the solvent was removed, the residue was purified by chromatography on silica using a hexane/ $\text{CH}_2\text{Cl}_2$  gradient. After removal of the solvent from the product-containing fractions, the compound was recrystallized from EtOH by slow evaporation, yielding large crystals suitable for X-ray crystallography (137 mg, 38%). IR (solid state, ATR)/cm<sup>-1</sup>:  $\nu(\text{C=C})$  2101. <sup>1</sup>H NMR ( $\text{CDCl}_3$ , 500 MHz,  $\delta$ /ppm): 1.15–1.27 (m, 18H, H<sup>9</sup>), 2.10–2.23 (m, 12H, H<sup>8</sup>), 2.45 (s, 6H, H<sup>7</sup>), 7.12 (d,  $J$  = 8.3 Hz, H<sup>5</sup>), 7.19 (d,  $J$  = 8.3 Hz, H<sup>4</sup>). <sup>13</sup>C{<sup>1</sup>H} NMR ( $\text{CDCl}_3$ , 126 MHz,  $\delta$ /ppm): 8.5 (m, C<sup>9</sup>), 16.47 (s, C<sup>7</sup>), 16.48 (pseudo-t (dd), apparent  $J$  = 17.6 Hz, C<sup>8</sup>), 108.1 (m, C<sup>1</sup>), 109.1 (br s, C<sup>2</sup>), 126.1 (s, C<sup>3</sup>), 126.9 (s, C<sup>5</sup>), 131.4 (s, C<sup>4</sup>), 134.6 (s, C<sup>6</sup>). <sup>31</sup>P{<sup>1</sup>H} NMR ( $\text{CDCl}_3$ , 200 MHz,  $\delta$ /ppm): 10.9 (s,  $J_{\text{Pt-P}}$  =

2372 Hz). MS (APCI-TOF)  $m/z$ : calcd for  $\text{C}_{30}\text{H}_{45}\text{P}_2\text{PtS}_2$  [M + H]<sup>+</sup> 726.2086; found 726.2087.

### Synthesis of 6b.



A solution of  $[\text{PtCl}_2(\text{PEt}_3)_2]$  (250 mg, 0.50 mmol), CuI (10 mg, 0.05 mmol), and 5-ethynyl-3,3-dimethyl-2,3-dihydrobenzo[b]-thiophene (**1b**; 210 mg, 1.12 mmol) in triethylamine (25 mL) was heated under reflux overnight. After the solvent was removed, the residue was extracted with hexane and the extract filtered through a silica plug. While the filtrate was concentrated under reduced pressure, the product precipitated as a yellow solid (187 mg, 46%). Crystals suitable for X-ray single-crystal crystallography were obtained by recrystallization from hot n-heptane or  $\text{CH}_2\text{Cl}_2$ /hexane. IR (solid state, ATR)/cm<sup>-1</sup>: 2098, 2085. <sup>1</sup>H NMR ( $\text{CDCl}_3$ , 500 MHz,  $\delta$ /ppm): 1.17–1.26 (m, 18H, H<sup>13</sup>), 1.35 (s, 12H, H<sup>11</sup>), 2.11–2.23 (m, 12H, H<sup>12</sup>), 3.15 (s, 4H, H<sup>10</sup>), 6.95 (d,  $J$  = 1.0 Hz, 2H, H<sup>8</sup>), 7.17 (d,  $J$  = 8.0 Hz, 2H, H<sup>5</sup>), 7.05 (dd,  $J$  = 8.0, 1.0 Hz, 2H, H<sup>4</sup>). <sup>13</sup>C{<sup>1</sup>H} NMR ( $\text{CDCl}_3$ , 126 MHz,  $\delta$ /ppm): 8.5 (s, C<sup>13</sup>), 16.5 (m, C<sup>12</sup>), 27.4 (m, C<sup>11</sup>), 47.3 (s, C<sup>9</sup>), 47.5 (s, C<sup>10</sup>), 106.7 (m, C<sup>1</sup>), 109.5 (s, C<sup>2</sup>), 122.0 (s, C<sup>5</sup>), 125.2 (br s, C<sup>3</sup> and C<sup>8</sup>), 130.2 (s, C<sup>4</sup>), 137.0 (s, C<sup>7</sup>), 147.7 (s, C<sup>6</sup>). <sup>31</sup>P{<sup>1</sup>H} NMR ( $\text{CDCl}_3$ , 202 MHz,  $\delta$ /ppm): 11.0 (s,  $J_{\text{PP}}$  = 2373 Hz). ESI(+)-MS  $m/z$ : calcd for  $\text{C}_{36}\text{H}_{52}\text{P}_2\text{PtS}_2$  806.2612 [M + H]<sup>+</sup>, found 806.2578. Anal. Calcd for  $\text{C}_{36}\text{H}_{52}\text{P}_2\text{PtS}_2$ : C, 53.59; H, 6.50. Found: C, 53.54; H, 6.62.

**Single-Crystal X-ray Diffraction Studies. General Conditions:** Single-Crystal X-ray Diffraction. Crystallographic data for the structures were collected at 100(2) K on an Oxford Diffraction Gemini diffractometer or an Oxford Diffraction Xcalibur X-Ray diffractometer. The data were corrected for Lorentz and polarization effects and absorption. The structures were solved by direct methods and refined against  $F^2$  with full-matrix least squares using the program suite SHELXL-97 or SHELXL-2014.<sup>99</sup> Anisotropic displacement parameters were employed for the non-hydrogen atoms. All hydrogen atoms were added at calculated positions and refined by use of a riding model with isotropic displacement parameters based on those of the parent atom. Crystallographic data for the structures reported in this paper can be found in the Supporting Information of this paper and have been deposited at the Cambridge Crystallographic Data Centre. Copies of the data with CCDC numbers 1938546–1938557 can be obtained free of charge via <https://www.ccdc.cam.ac.uk/structures/>, or from the Cambridge Crystallographic Data Centre, 12 Union Road, Cambridge CB2 1EZ, U.K (fax + 441223336033; email [deposit@ccdc.cam.ac.uk](mailto:deposit@ccdc.cam.ac.uk)).

**Crystal Data.** **1b:**  $\text{C}_{12}\text{H}_{12}\text{S}$ ,  $M$  = 188.28 g/mol, yellow needle,  $0.35 \times 0.19 \times 0.13$  mm<sup>3</sup>, orthorhombic, space group  $P2_12_12_1$  (No. 19),  $a$  = 6.79890(10) Å,  $b$  = 9.2508(2) Å,  $c$  = 15.8759(2) Å,  $V$  = 998.52(3) Å<sup>3</sup>,  $Z$  = 4,  $D_c$  = 1.252 g cm<sup>-3</sup>,  $\mu$  = 0.271 mm<sup>-1</sup>.  $F_{000}$  = 400, Mo  $\text{K}\alpha$  radiation,  $\lambda$  = 0.71073 Å,  $2\theta_{\text{max}}$  = 75.3°, 34907 reflections collected, 5177 unique ( $R_{\text{int}}$  = 0.0400), final GOF = 1.001,  $R_1$  = 0.0285,  $wR2$  = 0.0703,  $R$  indices based on 4835 reflections with  $I > 2\sigma(I)$ ,  $|\Delta\rho|_{\text{max}}$  = 0.38(5) e Å<sup>-3</sup>, 166 parameters, 0 restraints, absolute structure parameter = -0.002(17). CCDC number: 1938546.

**2b:**  $\text{C}_{24}\text{H}_{22}\text{S}_2$ ,  $M$  = 374.53 g/mol, pale yellow needle,  $0.242 \times 0.053 \times 0.051$  mm<sup>3</sup>, monoclinic, space group  $P2_1/n$  (No. 14),  $a$  = 7.0705(1) Å,  $b$  = 17.0655(2) Å,  $c$  = 16.2546(3) Å,  $\beta$  = 97.428(1)°,  $V$  = 1944.85(5) Å<sup>3</sup>,  $Z$  = 4,  $D_c$  = 1.279 g cm<sup>-3</sup>,  $\mu$  = 2.491 mm<sup>-1</sup>.  $F_{000}$  = 792, Cu  $\text{K}\alpha$  radiation,  $\lambda$  = 1.54178 Å,  $2\theta_{\text{max}}$  = 134.8°, 16578 reflections collected, 3478 unique ( $R_{\text{int}}$  = 0.0376), final GOF = 1.001,  $R_1$  = 0.0386,  $wR2$  = 0.0945,  $R$  indices based on 2863 reflections with  $I > 2\sigma(I)$ ,  $|\Delta\rho|_{\text{max}}$  = 0.27(5) e Å<sup>-3</sup>, 239 parameters, 0 restraints. CCDC number: 1938547.

**3b:** symmetry operation for generating equivalent atoms (A)  $-x - 2, 3 - y, 2 - z$ ;  $\text{C}_{30}\text{H}_{46}\text{S}_2$ ,  $M$  = 450.63 g/mol, colorless block, 0.40 ×

$0.30 \times 0.20$  mm<sup>3</sup>, monoclinic, space group  $P2_1/n$  (No. 14),  $a = 7.1172(3)$  Å,  $b = 10.4490(4)$  Å,  $c = 16.2683(7)$  Å,  $\beta = 94.466(3)^\circ$ ,  $V = 1206.16(9)$  Å<sup>3</sup>,  $Z = 2$ ,  $D_c = 1.241$  g cm<sup>-3</sup>,  $\mu = 0.236$  mm<sup>-1</sup>,  $F_{000} = 476$ , Mo K $\alpha$  radiation,  $\lambda = 0.71073$  Å,  $2\theta_{\max} = 52.00^\circ$ , 4736 reflections collected, 2362 unique ( $R_{\text{int}} = 0.0178$ ), final GOF = 1.037,  $R1 = 0.0330$ ,  $wR2 = 0.0844$ ,  $R$  indices based on 2173 reflections with  $I > 2\sigma(I)$ ,  $|\Delta\rho|_{\max} = 0.34(4)$  e Å<sup>-3</sup>, 147 parameters, 0 restraints. CCDC number: 1938548.

**4a:** symmetry operation for generating equivalent atoms (A)  $1 - x$ ,  $1 - y$ ,  $1 - z$ ;  $C_{70}H_{62}P_4RuS_2$ ,  $M = 1192.26$  g/mol, yellow needle,  $0.196 \times 0.042 \times 0.020$  mm<sup>3</sup>, triclinic, space group  $P\bar{1}$  (No. 2),  $a = 9.2372(3)$  Å,  $b = 13.0132(4)$  Å,  $c = 13.1830(4)$  Å,  $\alpha = 66.006(3)^\circ$ ,  $\beta = 88.900(2)^\circ$ ,  $\gamma = 77.291(2)^\circ$ ,  $V = 1407.87(8)$  Å<sup>3</sup>,  $Z = 1$ ,  $D_c = 1.406$  g cm<sup>-3</sup>,  $\mu = 4.354$  mm<sup>-1</sup>,  $F_{000} = 618$ , Cu K $\alpha$  radiation,  $\lambda = 1.54178$  Å,  $2\theta_{\max} = 134.5^\circ$ , 26946 reflections collected, 4988 unique ( $R_{\text{int}} = 0.0526$ ), final GOF = 1.000,  $R1 = 0.0315$ ,  $wR2 = 0.0782$ ,  $R$  indices based on 4293 reflections with  $I > 2\sigma(I)$ ,  $|\Delta\rho|_{\max} = 0.56(7)$  e Å<sup>-3</sup>, 350 parameters, 0 restraints. CCDC number: 1938549.

**4a·CH<sub>2</sub>Cl<sub>2</sub>:** selected bond properties summarized in Table 1; symmetry operation for generating equivalent atoms (A)  $1 - x$ ,  $1 - y$ ,  $1 - z$ ;  $C_{71}H_{64}Cl_2P_4RuS_2$ ,  $M = 1277.19$  g/mol, pale yellow plate,  $0.310 \times 0.210 \times 0.130$  mm<sup>3</sup>, monoclinic, space group  $P2_1/c$  (No. 14),  $a = 13.1788(2)$  Å,  $b = 22.8241(3)$  Å,  $c = 10.1272(1)$  Å,  $\beta = 102.857(1)^\circ$ ,  $V = 2969.83(7)$  Å<sup>3</sup>,  $Z = 2$ ,  $D_c = 1.428$  g cm<sup>-3</sup>,  $\mu = 0.576$  mm<sup>-1</sup>,  $F_{000} = 1320$ , Mo K $\alpha$  radiation,  $\lambda = 0.71073$  Å,  $2\theta_{\max} = 64.6^\circ$ , 63032 reflections collected, 10055 unique ( $R_{\text{int}} = 0.0461$ ), final GOF = 1.001,  $R1 = 0.0400$ ,  $wR2 = 0.0970$ ,  $R$  indices based on 8602 reflections with  $I > 2\sigma(I)$ ,  $|\Delta\rho|_{\max} = 2.5(1)$  e Å<sup>-3</sup>, 368 parameters, 0 restraints. CCDC number: 1938555.

**4b·CH<sub>2</sub>Cl<sub>2</sub>:** selected bond properties summarized in Table 1; symmetry operation for generating equivalent atoms (A)  $1 - x$ ,  $-y$ ,  $-z$ ;  $C_{77}H_{72}Cl_2P_4RuS_2$ ,  $M = 1357.31$  g/mol, orange needle,  $0.313 \times 0.066 \times 0.020$  mm<sup>3</sup>, triclinic, space group  $P\bar{1}$  (No. 2),  $a = 9.2078(3)$  Å,  $b = 13.1380(5)$  Å,  $c = 13.4746(6)$  Å,  $\alpha = 85.802(3)^\circ$ ,  $\beta = 87.326(3)^\circ$ ,  $\gamma = 83.114(3)^\circ$ ,  $V = 1612.77(11)$  Å<sup>3</sup>,  $Z = 1$ ,  $D_c = 1.398$  g cm<sup>-3</sup>,  $\mu = 4.614$  mm<sup>-1</sup>,  $F_{000} = 704$ , Cu K $\alpha$  radiation,  $\lambda = 1.54184$  Å,  $2\theta_{\max} = 134.6^\circ$ , 13061 reflections collected, 5693 unique ( $R_{\text{int}} = 0.0390$ ), final GOF = 1.036,  $R1 = 0.0385$ ,  $wR2 = 0.1008$ ,  $R$  indices based on 5114 reflections with  $I > 2\sigma(I)$ ,  $|\Delta\rho|_{\max} = 0.81(7)$  e Å<sup>-3</sup>, 435 parameters, 3 restraints. CCDC number: 1938555.

**4b·2CH<sub>2</sub>Cl<sub>2</sub>:** symmetry operation for generating equivalent atoms (A)  $2 - x$ ,  $1 - y$ ,  $1 - z$ ;  $C_{78}H_{74}Cl_4P_4RuS_2$ ,  $M = 1442.24$  g/mol, colorless needle,  $0.500 \times 0.070 \times 0.050$  mm<sup>3</sup>, monoclinic, space group  $P2_1/c$  (No. 14),  $a = 9.2236(2)$  Å,  $b = 13.0589(3)$  Å,  $c = 27.6792(7)$  Å,  $\beta = 94.976(2)^\circ$ ,  $V = 3321.40(13)$  Å<sup>3</sup>,  $Z = 2$ ,  $D_c = 1.442$  g cm<sup>-3</sup>,  $\mu = 0.602$  mm<sup>-1</sup>,  $F_{000} = 1492$ , Mo K $\alpha$  radiation,  $\lambda = 0.71073$  Å,  $2\theta_{\max} = 64.0^\circ$ , 69822 reflections collected, 11033 unique ( $R_{\text{int}} = 0.0769$ ), final GOF = 1.002,  $R1 = 0.0452$ ,  $wR2 = 0.0970$ ,  $R$  indices based on 8108 reflections with  $I > 2\sigma(I)$ ,  $|\Delta\rho|_{\max} = 0.8(1)$  e Å<sup>-3</sup>, 405 parameters, 0 restraints. CCDC number: 1938556.

**5a:**  $C_{42}H_{74}O_{12}P_4RuS_2$ ,  $M = 1060.08$  g/mol, colorless plate,  $0.386 \times 0.218 \times 0.137$  mm<sup>3</sup>, monoclinic, space group  $P2_1/n$  (No. 14),  $a = 11.7457(1)$  Å,  $b = 12.4496(2)$  Å,  $c = 35.9949(5)$  Å,  $\beta = 94.175(1)^\circ$ ,  $V = 5249.54(12)$  Å<sup>3</sup>,  $Z = 4$ ,  $D_c = 1.341$  g cm<sup>-3</sup>,  $\mu = 0.553$  mm<sup>-1</sup>,  $F_{000} = 2232$ , Mo K $\alpha$  radiation,  $\lambda = 0.71073$  Å,  $2\theta_{\max} = 63.9^\circ$ , 107960 reflections collected, 17459 unique ( $R_{\text{int}} = 0.0342$ ), final GOF = 1.003,  $R1 = 0.0325$ ,  $wR2 = 0.0797$ ,  $R$  indices based on 14902 reflections with  $I > 2\sigma(I)$ ,  $|\Delta\rho|_{\max} = 0.91(7)$  e Å<sup>-3</sup>, 574 parameters, 0 restraints. CCDC number: 1938551.

**5b:**  $C_{48}H_{82}O_{12}P_4RuS_2$ ,  $M = 1140.20$  g/mol, pale yellow needle,  $0.467 \times 0.317 \times 0.301$  mm<sup>3</sup>, orthorhombic, space group  $Pca2_1$  (No. 29),  $a = 24.8920(5)$  Å,  $b = 20.7702(4)$  Å,  $c = 11.2651(2)$  Å,  $V = 5824.19(19)$  Å<sup>3</sup>,  $Z = 4$ ,  $D_c = 1.300$  g cm<sup>-3</sup>,  $\mu = 0.504$  mm<sup>-1</sup>,  $F_{000} = 2408$ , Mo K $\alpha$  radiation,  $\mu = 0.71073$  Å,  $2\theta_{\max} = 65.4^\circ$ , 35710 reflections collected, 18467 unique ( $R_{\text{int}} = 0.0320$ ), final GOF = 1.006,  $R1 = 0.0577$ ,  $wR2 = 0.1342$ ,  $R$  indices based on 13869 reflections with  $I > 2\sigma(I)$ ,  $|\Delta\rho|_{\max} = 2.3(1)$  e Å<sup>-3</sup>, 624 parameters, 18 restraints, absolute structure parameter  $-0.053(13)$ .<sup>100</sup> CCDC number: 1938552.

**6a:** symmetry operation for generating equivalent atoms (A)  $1 - x$ ,  $1 - y$ ,  $1 - z$ ;  $C_{30}H_{44}P_2PtS_2$ ,  $M = 725.80$  g/mol, yellow prism,  $0.659 \times 0.405 \times 0.331$  mm<sup>3</sup>, triclinic, space group  $P\bar{1}$  (No. 2),  $a = 8.7144(3)$  Å,  $b = 9.4046(4)$  Å,  $c = 11.1777(4)$  Å,  $\alpha = 97.754(3)^\circ$ ,  $\beta = 102.336(3)^\circ$ ,  $\gamma = 116.694(4)^\circ$ ,  $V = 771.05(6)$  Å<sup>3</sup>,  $Z = 1$ ,  $D_c = 1.563$  g cm<sup>-3</sup>,  $\mu = 4.806$  mm<sup>-1</sup>,  $F_{000} = 364$ , Mo K $\alpha$  radiation,  $\lambda = 0.71073$  Å,  $2\theta_{\max} = 75.3^\circ$ , 14871 reflections collected, 7739 unique ( $R_{\text{int}} = 0.0171$ ), final GOF = 1.044,  $R1 = 0.0153$ ,  $wR2 = 0.0366$ ,  $R$  indices based on 7739 reflections with  $I > 2\sigma(I)$ ,  $|\Delta\rho|_{\max} = 1.2(1)$  e Å<sup>-3</sup>, 164 parameters, 0 restraints. CCDC number: 1938553.

**6b:** symmetry operation for generating equivalent atoms (A)  $-x$ ,  $1 - y$ ,  $1 - z$ ;  $C_{36}H_{52}P_2PtS_2$ ,  $M = 805.92$ , yellow block,  $0.267 \times 0.196 \times 0.094$  mm<sup>3</sup>, triclinic, space group  $P\bar{1}$  (No. 2),  $a = 13.4351(3)$  Å,  $b = 13.8251(3)$  Å,  $c = 15.8416(3)$  Å,  $\alpha = 83.638(2)^\circ$ ,  $\beta = 66.108(2)^\circ$ ,  $\gamma = 80.253(2)^\circ$ ,  $V = 2648.56(11)$  Å<sup>3</sup>,  $Z = 3$ ,  $D_c = 1.516$  g cm<sup>-3</sup>,  $\mu = 4.206$  mm<sup>-1</sup>,  $F_{000} = 1224$ , Mo K $\alpha$  radiation,  $\lambda = 0.71073$  Å,  $2\theta_{\max} = 64.7^\circ$ , 54728 reflections collected, 17368 unique ( $R_{\text{int}} = 0.0378$ ), final GOF = 1.001,  $R1 = 0.0336$ ,  $wR2 = 0.0734$ ,  $R$  indices based on 14058 reflections with  $I > 2\sigma(I)$ ,  $|\Delta\rho|_{\max} = 4.5(1)$  e Å<sup>-3</sup>, 637 parameters, 31 restraints. CCDC number: 1938554.

**6b (polymorph):** symmetry operation for generating equivalent atoms (A)  $-x$ ,  $-y$ ,  $1 - z$ ;  $C_{36}H_{52}P_2PtS_2$ ,  $M = 805.92$  g/mol, pale orange plate,  $0.354 \times 0.121 \times 0.032$  mm<sup>3</sup>, triclinic, space group  $P\bar{1}$  (No. 2),  $a = 8.2254(13)$  Å,  $b = 8.3524(8)$  Å,  $c = 13.8460(16)$  Å,  $\alpha = 83.493(9)^\circ$ ,  $\beta = 80.404(12)^\circ$ ,  $\gamma = 71.421(12)^\circ$ ,  $V = 887.2(2)$  Å<sup>3</sup>,  $Z = 1$ ,  $D_c = 1.508$  g cm<sup>-3</sup>,  $\mu = 9.510$  mm<sup>-1</sup>,  $F_{000} = 408$ , Cu K $\alpha$  radiation,  $\lambda = 1.54184$  Å,  $2\theta_{\max} = 134.8^\circ$ , 5438 reflections collected, 3047 unique ( $R_{\text{int}} = 0.0631$ ), final GOF = 1.090,  $R1 = 0.1047$ ,  $wR2 = 0.2811$ ,  $R$  indices based on 2651 reflections with  $I > 2\sigma(I)$ ,  $|\Delta\rho|_{\max} = 3.4(3)$  e Å<sup>-3</sup>, 250 parameters, 100 restraints. CCDC number: 1938557.

## ASSOCIATED CONTENT

### Supporting Information

The Supporting Information is available free of charge at <https://pubs.acs.org/doi/10.1021/acs.organomet.0c00685>.

Additional plots of crystallographically determined molecular structures and refinement information, plots and composition of selected molecular orbitals, and plots of UV-vis spectra of 1a,b–6a,b (PDF)

### Accession Codes

CCDC 1938546–1938557 contain the supplementary crystallographic data for this paper. These data can be obtained free of charge via [www.ccdc.cam.ac.uk/data\\_request/cif](http://www.ccdc.cam.ac.uk/data_request/cif), or by emailing [data\\_request@ccdc.cam.ac.uk](mailto:data_request@ccdc.cam.ac.uk), or by contacting The Cambridge Crystallographic Data Centre, 12 Union Road, Cambridge CB2 1EZ, UK; fax: +44 1223 336033.

## AUTHOR INFORMATION

### Corresponding Author

**Paul J. Low** – School of Molecular Sciences, University of Western Australia, Crawley, Western Australia 6009, Australia;  [orcid.org/0000-0003-1136-2296](http://orcid.org/0000-0003-1136-2296); Email: [paul.low@uwa.edu.au](mailto:paul.low@uwa.edu.au)

### Authors

**Masnun Naher** – School of Molecular Sciences, University of Western Australia, Crawley, Western Australia 6009, Australia

**Sören Bock** – School of Molecular Sciences, University of Western Australia, Crawley, Western Australia 6009, Australia

**Zakary M. Langtry** – School of Molecular Sciences, University of Western Australia, Crawley, Western Australia 6009, Australia

Kieran M. O'Malley — School of Molecular Sciences,  
University of Western Australia, Crawley, Western Australia  
6009, Australia

Alexandre N. Sobolev — School of Molecular Sciences,  
University of Western Australia, Crawley, Western Australia  
6009, Australia

Brian W. Skelton — School of Molecular Sciences, University of  
Western Australia, Crawley, Western Australia 6009,  
Australia

Marcus Korb — School of Molecular Sciences, University of  
Western Australia, Crawley, Western Australia 6009,  
Australia

Complete contact information is available at:  
<https://pubs.acs.org/10.1021/acs.organomet.0c00685>

### Author Contributions

†M.N. and S.B. contributed equally.

### Notes

The authors declare no competing financial interest.

### ACKNOWLEDGMENTS

This paper is dedicated to Professor Jean-René Hamon on the occasion of his 65th birthday, in celebration of his many achievements in chemistry and with thanks for his friendship. The Australian Research Council (ARC) is thanked for financial support under the Discovery Program (DP190100073; DP190100074). M.N. holds a Forrest Scholarship from the Forrest Research Foundation. M.K. holds a Forrest Fellowship from the Forrest Research Foundation. S.B. held an International Postgraduate Research Scholarship and Scholarship for International Research Fees from the University of Western Australia and Faculty of Science. The authors gratefully acknowledge the facilities and the scientific and technical assistance of Microscopy Australian at the Centre for Microscopy, Characterisation & Analysis, The University of Western Australia, a facility funded by the University and State and Commonwealth Governments.

### REFERENCES

- (1) Wang, L.; Wang, L.; Zhang, L.; Xiang, D. Advance of Mechanically Controllable Break Junction for Molecular Electronics. *Top. Curr. Chem.* **2017**, *375*, 61.
- (2) Wang, K.; Xu, B. Q. Modulation and Control of Charge Transport Through Single-Molecule Junctions. *Top. Curr. Chem.* **2017**, *375*, 17.
- (3) Vilan, A.; Aswal, D.; Cahen, D. Large-Area, Ensemble Molecular Electronics: Motivation and Challenges. *Chem. Rev.* **2017**, *117*, 4248–4286.
- (4) Huang, C. C.; Rudnev, A. V.; Hong, W. J.; Wandlowski, T. Break junction under electrochemical gating: testbed for single-molecule electronics. *Chem. Soc. Rev.* **2015**, *44*, 889–901.
- (5) Kiguchi, M.; Kaneko, S. Single molecule bridging between metal electrodes. *Phys. Chem. Chem. Phys.* **2013**, *15*, 2253–2267.
- (6) Leary, E.; La Rosa, A.; Gonzalez, M. T.; Rubio-Bollinger, G.; Agrait, N.; Martin, N. Incorporating single molecules into electrical circuits. The role of the chemical anchoring group. *Chem. Soc. Rev.* **2015**, *44*, 920–942.
- (7) Xiang, D.; Wang, X. L.; Jia, C. C.; Lee, T.; Guo, X. F. Molecular-Scale Electronics: From Concept to Function. *Chem. Rev.* **2016**, *116*, 4318–4440.
- (8) Su, T. A.; Neupane, M.; Steigerwald, M. L.; Venkataraman, L.; Nuckolls, C. Chemical principles of single-molecule electronics. *Nat. Rev. Mater.* **2016**, *1*, 1–15.
- (9) Schwarz, F.; Kastlunger, G.; Lissel, F.; Riel, H.; Venkatesan, K.; Berke, H.; Stadler, R.; Lortscher, E. High-Conductive Organometallic Molecular Wires with Delocalized Electron Systems Strongly Coupled to Metal Electrodes. *Nano Lett.* **2014**, *14*, 5932–5940.
- (10) Lissel, F.; Schwarz, F.; Blacque, O.; Riel, H.; Lortscher, E.; Venkatesan, K.; Berke, H. Organometallic Single-Molecule Electronics: Tuning Electron Transport through  $X(\text{diphosphine})_2\text{FeC}_4\text{Fe}(\text{diphosphine})_2X$  Building Blocks by Varying the Fe-X-Au Anchoring Scheme from Coordinative to Covalent. *J. Am. Chem. Soc.* **2014**, *136*, 14560–14569.
- (11) Duan, P.; Liu, J. Y.; Wang, J. Y.; Chen, L. C.; Wang, F.; Zhang, Q. C.; Hong, W.; Chen, Z. N. Modulation of the conductance in platinum(II) bis(acetylidyne) molecules through “gating” metal ions. *J. Mater. Chem. C* **2019**, *7*, 7259–7266.
- (12) Davidson, R.; Al-Owaedi, O. A.; Milan, D. C.; Zeng, Q.; Tory, J.; Hartl, F.; Higgins, S. J.; Nichols, R. J.; Lambert, C. J.; Low, P. J. Effects of Electrode-Molecule Binding and Junction Geometry on the Single-Molecule Conductance of bis-2,2 ‘:6 ‘,2“-Terpyridine-based Complexes. *Inorg. Chem.* **2016**, *55*, 2691–2700.
- (13) Davidson, R.; Liang, J. H.; Milan, D. C.; Mao, B. W.; Nichols, R. J.; Higgins, S. J.; Yufit, D. S.; Beeby, A.; Low, P. J. Synthesis, Electrochemistry, and Single-Molecule Conductance of Bimetallic 2,3,5,6-Tetra-(pyridine-2-yl)pyrazine-Based Complexes. *Inorg. Chem.* **2015**, *54*, 5487–5494.
- (14) Zhao, X. T.; Huang, C. C.; Gulcur, M.; Batsanov, A. S.; Baghernejad, M.; Hong, W. J.; Bryce, M. R.; Wandlowski, T. Oligo(aryleneethynylene)s with Terminal Pyridyl Groups: Synthesis and Length Dependence of the Tunneling-to-Hopping Transition of Single-Molecule Conductances. *Chem. Mater.* **2013**, *25*, 4340–4347.
- (15) Quinn, J. R.; Foss, F. W.; Venkataraman, L.; Breslow, R. Oxidation potentials correlate with conductivities of aromatic molecular wires. *J. Am. Chem. Soc.* **2007**, *129*, 12376–12377.
- (16) Kastlunger, G.; Stadler, R. Density functional theory based direct comparison of coherent tunneling and electron hopping in redox-active single-molecule junctions. *Phys. Rev. B: Condens. Matter Mater. Phys.* **2015**, *91*, 125410.
- (17) Zhang, J. D.; Kuznetsov, A. M.; Medvedev, I. G.; Chi, Q. J.; Albrecht, T.; Jensen, P. S.; Ulstrup, J. Single-molecule electron transfer in electrochemical environments. *Chem. Rev.* **2008**, *108*, 2737–2791.
- (18) Osorio, H. M.; Catarelli, S.; Cea, P.; Gluyas, J. B. G.; Hartl, F.; Higgins, S. J.; Leary, E.; Low, P. J.; Martin, S.; Nichols, R. J.; Tory, J.; Ulstrup, J.; Vezzoli, A.; Milan, D. C.; Zeng, Q. Electrochemical Single-Molecule Transistors with Optimized Gate Coupling. *J. Am. Chem. Soc.* **2015**, *137*, 14319–14328.
- (19) Chappell, S.; Brooke, C.; Nichols, R. J.; Cook, L. J. K.; Halcrow, M.; Ulstrup, J.; Higgins, S. J. Evidence for a hopping mechanism in metall single molecule metal junctions involving conjugated metal-terpyridyl complexes; potential-dependent conductances of complexes  $[\text{M}(\text{pyterp})_2]^{2+}$  ( $\text{M} = \text{Co}$  and  $\text{Fe}$ ; pyterp = 4 ‘-(pyridin-4-yl)-2,2 ‘:6 ‘,2“-terpyridine) in ionic liquid. *Faraday Discuss.* **2016**, *193*, 113–131.
- (20) Lambert, C. J. Basic concepts of quantum interference and electron transport in single-molecule electronics. *Chem. Soc. Rev.* **2015**, *44*, 875–888.
- (21) Higgins, S. J.; Nichols, R. J. Metallmoleculemetal junction studies of organometallic and coordination complexes; What can transition metals do for molecular electronics? *Polyhedron* **2018**, *140*, 25–34.
- (22) Milan, D. C.; Vezzoli, A.; Planje, I. J.; Low, P. J. Metal bis(acetylidyne) complex molecular wires: concepts and design strategies. *Dalton Trans.* **2018**, *47*, 14125–14138.
- (23) Tanaka, Y.; Kiguchi, M.; Akita, M. Inorganic and Organometallic Molecular Wires for Single-Molecule Devices. *Chem. - Eur. J.* **2017**, *23*, 4741–4749.
- (24) Rigaut, S. Metal complexes in molecular junctions. *Dalton Trans.* **2013**, *42*, 15859–15863.
- (25) Low, P. J. Metal complexes in molecular electronics: progress and possibilities. *Dalton Trans.* **2005**, 2821–2824.

- (26) Ruben, M.; Landa, A.; Lortscher, E.; Riel, H.; Mayor, M.; Gorls, H.; Weber, H. B.; Arnold, A.; Evers, F. Charge Transport Through a Cardan-Joint Molecule. *Small* **2008**, *4*, 2229–2235.
- (27) Tanaka, Y.; Kato, Y.; Tada, T.; Fujii, S.; Kiguchi, M.; Akita, M. “Doping” of Polyyne with an Organometallic Fragment Leads to Highly Conductive Metallapolyyne Molecular Wire. *J. Am. Chem. Soc.* **2018**, *140*, 10080–10084.
- (28) Schwarz, F.; Kastlunger, G.; Lissel, F.; Egler-Lucas, C.; Semenov, S. N.; Venkatesan, K.; Berke, H.; Stadler, R.; Lortscher, E. Field-induced conductance switching by charge-state alternation in organometallic single-molecule junctions. *Nat. Nanotechnol.* **2016**, *11*, 170–176.
- (29) Frisenda, R.; Harzmann, G. D.; Gil, J. A. C.; Thijssen, J. M.; Mayor, M.; van der Zant, H. S. J. Stretching-Induced Conductance Increase in a Spin-Crossover Molecule. *Nano Lett.* **2016**, *16*, 4733–4737.
- (30) Harzmann, G. D.; Frisenda, R.; van der Zant, H. S. J.; Mayor, M. Single-Molecule Spin Switch Based on Voltage-Triggered Distortion of the Coordination Sphere. *Angew. Chem., Int. Ed.* **2015**, *54*, 13425–13430.
- (31) Albrecht, T.; Guckian, A.; Kuznetsov, A. M.; Vos, J. G.; Ulstrup, J. Mechanism of electrochemical charge transport in individual transition metal complexes. *J. Am. Chem. Soc.* **2006**, *128*, 17132–17138.
- (32) Kuznetsov, A. M.; Ulstrup, J. Mechanisms of in situ scanning tunnelling microscopy of organized redox molecular assemblies. *J. Phys. Chem. A* **2000**, *104*, 11531–11540.
- (33) Albrecht, T.; Guckian, A.; Ulstrup, J.; Vos, J. G. Transistor-like behavior of transition metal complexes. *Nano Lett.* **2005**, *5*, 1451–1455.
- (34) Kaliginedi, V.; Rudnev, A. V.; Moreno-Garcia, P.; Baghernejad, M.; Huang, C. C.; Hong, W. J.; Wandlowski, T. Promising anchoring groups for single-molecule conductance measurements. *Phys. Chem. Chem. Phys.* **2014**, *16*, 23529–23539.
- (35) Dell, E. J.; Capozzi, B.; Xia, J. L.; Venkataraman, L.; Campos, L. M. Molecular length dictates the nature of charge carriers in single-molecule junctions of oxidized oligothiophenes. *Nat. Chem.* **2015**, *7*, 209–214.
- (36) Moreno-Garcia, P.; Gulcur, M.; Manrique, D. Z.; Pope, T.; Hong, W. J.; Kaliginedi, V.; Huang, C. C.; Batsanov, A. S.; Bryce, M. R.; Lambert, C.; Wandlowski, T. Single-Molecule Conductance of Functionalized Oligoynes: Length Dependence and Junction Evolution. *J. Am. Chem. Soc.* **2013**, *135*, 12228–12240.
- (37) Liu, J. Y.; Zhao, X. T.; Al-Galiby, Q.; Huang, X. Y.; Zheng, J. T.; Li, R. H.; Huang, C. C.; Yang, Y.; Shi, J.; Manrique, D. Z.; Lambert, C. J.; Bryce, M. R.; Hong, W. J. Radical-Enhanced Charge Transport in Single-Molecule Phenothiazine Electrical Junctions. *Angew. Chem., Int. Ed.* **2017**, *56*, 13061–13065.
- (38) Li, Y. H.; Baghernejad, M.; Qusiy, A. G.; Manrique, D. Z.; Zhang, G. X.; Hamill, J.; Fu, Y. C.; Broekmann, P.; Hong, W. J.; Wandlowski, T.; Zhang, D. Q.; Lambert, C. Three-State Single-Molecule Naphthalenediimide Switch: Integration of a Pendant Redox Unit for Conductance Tuning. *Angew. Chem., Int. Ed.* **2015**, *54*, 13586–13589.
- (39) Dekkiche, H.; Gemma, A.; Tabatabaei, F.; Batsanov, A. S.; Niehaus, T.; Gotsmann, B.; Bryce, M. R. Electronic conductance and thermopower of single-molecule junctions of oligo(phenyleneethynylene) derivatives. *Nanoscale* **2020**, *12*, 18908–18917.
- (40) Ozawa, H.; Baghernejad, M.; Al-Owaedi, O. A.; Kaliginedi, V.; Nagashima, T.; Ferrer, J.; Wandlowski, T.; Garcia-Suarez, V. M.; Broekmann, P.; Lambert, C. J.; Haga, M. Synthesis and Single-Molecule Conductance Study of Redox-Active Ruthenium Complexes with Pyridyl and Dihydrobenzo[b]thiophene Anchoring Groups. *Chem. - Eur. J.* **2016**, *22*, 12732–12740.
- (41) Yan, F.; Chen, F.; Wu, X. H.; Luo, J.; Zhou, X. S.; Horsley, J. R.; Abell, A. D.; Yu, J. X.; Jin, S.; Mao, B. W. Unique Metal Cation Recognition via Crown Ether-Derivatized Oligo(phenyleneethynylene) Molecular Junction. *J. Phys. Chem. C* **2020**, *124*, 8496–8503.
- (42) Meisner, J. S.; Sedbrook, D. F.; Krikorian, M.; Chen, J.; Sattler, A.; Carnes, M. E.; Murray, C. B.; Steigerwald, M.; Nuckolls, C. Functionalizing molecular wires: a tunable class of  $\alpha,\omega$ -diphenyl- $\mu,\nu$ -dicyano-oligoenes. *Chem. Sci.* **2012**, *3*, 1007–1014.
- (43) Meisner, J. S.; Kamenetska, M.; Krikorian, M.; Steigerwald, M. L.; Venkataraman, L.; Nuckolls, C. A Single-Molecule Potentiometer. *Nano Lett.* **2011**, *11*, 1575–1579.
- (44) Bock, S.; Low, P. J. A Safe and Simple Synthesis of 1,4-Bis(trimethylsilyl) buta-1,3-diyne. *Aust. J. Chem.* **2018**, *71*, 307–310.
- (45) Navale, B. S.; Bhat, R. G. Copper(I) iodide-DMAP catalyzed homo- and heterocoupling of terminal alkynes. *RSC Adv.* **2013**, *3*, 5220–5226.
- (46) Batsanov, A. S.; Collings, J. C.; Fairlamb, I. J. S.; Holland, J. P.; Howard, J. A. K.; Lin, Z. Y.; Marder, T. B.; Parsons, A. C.; Ward, R. M.; Zhu, J. Requirement for an oxidant in Pd/Cu co-catalyzed terminal alkyne homocoupling give symmetrical 1,4-disubstituted 1,3-diyne. *J. Org. Chem.* **2005**, *70*, 703–706.
- (47) Milan, D. C.; Al-Owaedi, O. A.; Oerthel, M. C.; Marques-Gonzalez, S.; Brooke, R. J.; Bryce, M. R.; Cea, P.; Ferrer, J.; Higgins, S. J.; Lambert, C. J.; Low, P. J.; Manrique, D. Z.; Martin, S.; Nichols, R. J.; Schwarzacher, W.; Garcia-Suarez, V. M. Solvent Dependence of the Single Molecule Conductance of Oligoynes-Based Molecular Wires. *J. Phys. Chem. C* **2016**, *120*, 15666–15674.
- (48) Liu, K.; Wang, X. H.; Wang, F. S. Probing Charge Transport of Ruthenium-Complex-Based Molecular Wires at the Single-Molecule Level. *ACS Nano* **2008**, *2*, 2315–2323.
- (49) Lu, Q.; Liu, K.; Zhang, H. M.; Du, Z. B.; Wang, X. H.; Wang, F. S. From Tunneling to Hopping: A Comprehensive Investigation of Charge Transport Mechanism in Molecular Junctions Based on Oligo(p-phenylene ethynylene)s. *ACS Nano* **2009**, *3*, 3861–3868.
- (50) Frisenda, R.; Tarkuc, S.; Galan, E.; Perrin, M. L.; Eelkema, R.; Grozema, F. C.; van der Zant, H. S. J. Electrical properties and mechanical stability of anchoring groups for single-molecule electronics. *Beilstein J. Nanotechnol.* **2015**, *6*, 1558–1567.
- (51) Wei, Z. M.; Hansen, T.; Santella, M.; Wang, X. T.; Parker, C. R.; Jiang, X. B.; Li, T.; Glyvradal, M.; Jenum, K.; Glibstrup, E.; Bovet, N.; Wang, X. W.; Hu, W. P.; Solomon, G. C.; Nielsen, M. B.; Qiu, X. H.; Bjornholm, T.; Norgaard, K.; Laursen, B. W. Molecular Heterojunctions of Oligo(phenylene ethynylene)s with Linear to Cruciform Framework. *Adv. Funct. Mater.* **2015**, *25*, 1700–1708.
- (52) Zheng, J. T.; Yan, R. W.; Tian, J. H.; Liu, J. Y.; Pei, L. Q.; Wu, D. Y.; Dai, K.; Yang, Y.; Jin, S.; Hong, W. J.; Tian, Z. Q. Electrochemically assisted mechanically controllable break junction studies on the stacking configurations of oligo(phenylene ethynylene)s molecular junctions. *Electrochim. Acta* **2016**, *200*, 268–275.
- (53) Masai, H.; Fujihara, T.; Tsuji, Y.; Terao, J. Programmed Synthesis of Molecular Wires with Fixed Insulation and Defined Length Based on Oligo(phenylene ethynylene) and Permethylated-Cyclodextrins. *Chem. - Eur. J.* **2017**, *23*, 15073–15079.
- (54) Miao, R. J.; Xu, H. L.; Skripnik, M.; Cui, L. J.; Wang, K.; Pedersen, K. G. L.; Leijnse, M.; Pauly, F.; Warnmark, K.; Meyhofer, E.; Reddy, P.; Linke, H. Influence of Quantum Interference on the Thermoelectric Properties of Molecular Junctions. *Nano Lett.* **2018**, *18*, 5666–5672.
- (55) Rodriguez-Gonzalez, S.; Xie, Z.; Galangau, O.; Selvanathan, P.; Norel, L.; Van Dyck, C.; Costuas, K.; Frisbie, C. D.; Rigaut, S.; Cornil, J. HOMO Level Pinning in Molecular Junctions: Joint Theoretical and Experimental Evidence. *J. Phys. Chem. Lett.* **2018**, *9*, 2394–2403.
- (56) Herrer, L.; Gonzalez-Orive, A.; Marques-Gonzalez, S.; Martin, S.; Nichols, R. J.; Serrano, J. L.; Low, P. J.; Cea, P. Electrically transmissive alkyne-anchored monolayers on gold. *Nanoscale* **2019**, *11*, 7976–7985.
- (57) Liu, Y. Q.; Zhong, M. Z.; Downey, E. F.; Chen, X. Y.; Li, T.; Norgaard, K.; Wei, Z. M. Temperature dependence of charge transport in solid-state molecular junctions based on oligo(phenylene ethynylene)s. *Nanotechnology* **2020**, *31*, 164001.
- (58) Liu, J. Y.; Zhao, X. T.; Zheng, J. T.; Huang, X. Y.; Tang, Y. Z.; Wang, F.; Li, R. H.; Pi, J. C.; Huang, C. C.; Wang, L.; Yang, Y.; Shi, J.;

- Mao, B. W.; Tian, Z. Q.; Bryce, M. R.; Hong, W. J. Transition from Tunneling Leakage Current to Molecular Tunneling in Single-Molecule Junctions. *Chem.* **2019**, *5*, 390–401.
- (59) Nguyen, P.; Zheng, Y. A.; Agocs, L.; Lesley, G.; Marder, T. B. Synthesis of Symmetrical and Unsymmetric 1,4-Bis(P-R-Phenylethynyl)BenzeneS Via Palladium Copper-Catalyzed Cross-Coupling and Comments on the Coupling of Aryl Halides with Terminal Alkynes. *Inorg. Chim. Acta* **1994**, *220*, 289–296.
- (60) Miguel, D.; de Cienfuegos, L. A.; Martin-Lasanta, A.; Morcillo, S. P.; Zotti, L. A.; Leary, E.; Burkle, M.; Asai, Y.; Jurado, R.; Cardenas, D. J.; Rubio-Bollinger, G.; Agrait, N.; Cuerva, J. M.; Gonzalez, M. T. Toward Multiple Conductance Pathways with Heterocycle-Based Oligo(phenyleneethynylene) Derivatives. *J. Am. Chem. Soc.* **2015**, *137*, 13818–13826.
- (61) Marques-Gonzalez, S.; Yufit, D. S.; Howard, J. A. K.; Martin, S.; Osorio, H. M.; Garcia-Suarez, V. M.; Nichols, R. J.; Higgins, S. J.; Cea, P.; Low, P. J. Simplifying the conductance profiles of molecular junctions: the use of the trimethylsilylethynyl moiety as a molecule-gold contact. *Dalton Trans.* **2013**, *42*, 338–341.
- (62) Al-Owaedi, O. A.; Milan, D. C.; Oerthel, M. C.; Bock, S.; Yufit, D. S.; Howard, J. A. K.; Higgins, S. J.; Nichols, R. J.; Lambert, C. J.; Bryce, M. R.; Low, P. J. Experimental and Computational Studies of the Single-Molecule Conductance of Ru(II) and Pt(II) trans-Bis(acetylidyne) Complexes. *Organometallics* **2016**, *35*, 2944–2954.
- (63) Bock, S.; Al-Owaedi, O. A.; Eaves, S. G.; Milan, D. C.; Lemmer, M.; Skelton, B. W.; Osorio, H. M.; Nichols, R. J.; Higgins, S. J.; Cea, P.; Long, N. J.; Albrecht, T.; Martin, S.; Lambert, C. J.; Low, P. J. Single-Molecule Conductance Studies of Organometallic Complexes Bearing 3-Thienyl Contacting Groups. *Chem. - Eur. J.* **2017**, *23*, 2133–2143.
- (64) Ezquerra, R.; Eaves, S. G.; Bock, S.; Skelton, B. W.; Perez-Murano, F.; Cea, P.; Martin, S.; Low, P. J. New routes to organometallic molecular junctions via a simple thermal processing protocol. *J. Mater. Chem. C* **2019**, *7*, 6630–6640.
- (65) Luo, L.; Benameur, A.; Brignou, P.; Choi, S. H.; Rigaut, S.; Frisbie, C. D. Length and Temperature Dependent Conduction of Ruthenium-Containing Redox-Active Molecular Wires. *J. Phys. Chem. C* **2011**, *115*, 19955–19961.
- (66) Kim, B.; Beebe, J. M.; Olivier, C.; Rigaut, S.; Touchard, D.; Kushmerick, J. G.; Zhu, X. Y.; Frisbie, C. D. Temperature and length dependence of charge transport in redox-active molecular wires incorporating ruthenium(II) bis(I-arylacetylidyne) complexes. *J. Phys. Chem. C* **2007**, *111*, 7521–7526.
- (67) Sugimoto, K.; Tanaka, Y.; Fujii, S.; Tada, T.; Kiguchi, M.; Akita, M. Organometallic molecular wires as versatile modules for energy-level alignment of the metal-molecule-metal junction. *Chem. Commun.* **2016**, *S2*, 5796–5799.
- (68) Zhang, L. Y.; Duan, P.; Wang, J. Y.; Zhang, Q. C.; Chen, Z. N. Ruthenium(II) as Conductive Promoter To Alleviate Conductance Attenuation in Oligoynyl Chains. *J. Phys. Chem. C* **2019**, *123* (9), 5282–5288.
- (69) Marques-Gonzalez, S.; Parthey, M.; Yufit, D. S.; Howard, J. A. K.; Kaupp, M.; Low, P. J. Combined Spectroscopic and Quantum Chemical Study of [trans-Ru(C<sub>6</sub>C<sub>6</sub>H<sub>4</sub>R<sup>1</sup>)<sub>4</sub>](dppe)<sub>2</sub>]<sup>n+</sup> and [trans-Ru(C<sub>6</sub>C<sub>6</sub>H<sub>4</sub>R<sup>1</sup>)<sub>4</sub>](C<sub>6</sub>C<sub>6</sub>H<sub>4</sub>R<sup>2</sup>)<sub>4</sub>](dppe)<sub>2</sub>]<sup>n+</sup> (n = 0, 1) Complexes: Interpretations beyond the Lowest Energy Conformer Paradigm. *Organometallics* **2014**, *33*, 4947–4963.
- (70) Olivier, C.; Kim, B.; Touchard, D.; Rigaut, S. Redox-active molecular wires incorporating ruthenium(II) 7-arylacetylidyne complexes for molecular electronics. *Organometallics* **2008**, *27* (4), S09–S18.
- (71) Lau, K.; Barlow, A.; Moxey, G. J.; Li, Q.; Liu, Y.; Humphrey, M. G.; Cifuentes, M. P.; Frankcombe, T. J.; Stranger, R. Large electric-field-induced strain in centrosymmetric crystals of a dipolar ruthenium alkynyl complex. *Phys. Chem. Chem. Phys.* **2015**, *17*, 10781–10785.
- (72) Al-Owaedi, O. A.; Bock, S.; Milan, D. C.; Oerthel, M. C.; Inkpen, M. S.; Yufit, D. S.; Sobolev, A. N.; Long, N. J.; Albrecht, T.; Higgins, S. J.; Bryce, M. R.; Nichols, R. J.; Lambert, C. J.; Low, P. J. Insulated molecular wires: inhibiting orthogonal contacts in metal complex based molecular junctions. *Nanoscale* **2017**, *9*, 9902–9912.
- (73) Eaves, S. G.; Skelton, B. W.; Low, P. J. Syntheses and molecular structures of *trans*-bis(alkynyl) tetrakis-triethylphosphite ruthenium complexes. *J. Organomet. Chem.* **2017**, *847*, 242–250.
- (74) Mayor, M.; von Hanisch, C.; Weber, H. B.; Reichert, J.; Beckmann, D. A *trans*-platinum(II) complex as a single-molecule insulator. *Angew. Chem., Int. Ed.* **2002**, *41*, 1183–1186.
- (75) Schull, T. L.; Kushmerick, J. G.; Patterson, C. H.; George, C.; Moore, M. H.; Pollack, S. K.; Shashidhar, R. Ligand effects on charge transport in platinum(II) acetylides. *J. Am. Chem. Soc.* **2003**, *125*, 3202–3203.
- (76) Duan, P.; Liu, J. Y.; Wang, J. Y.; Qu, K.; Cai, S. N.; Wang, F.; Chen, L. C.; Huang, X. Y.; Li, R. H.; Shi, J.; Zhang, Q. C.; Hong, W. J.; Chen, Z. N. Enhancing single-molecule conductance of platinum(II) complexes through synergistic aromaticity-assisted structural asymmetry. *Sci. China: Chem.* **2020**, *63*, 467–474.
- (77) Juvenal, F.; Bonnot, A.; Fortin, D.; Harvey, P. D. The *trans*-Bis(p-thioetherphenylacetylidyne)bis(phosphine)platinum(II) Ligands: A Step towards Predictability and Crystal Design. *ACS Omega* **2017**, *2*, 7433–7443.
- (78) Dai, C. Y.; Yuan, Z.; Collings, J. C.; Fasina, T. M.; Thomas, R. L.; Roscoe, K. P.; Stimson, L. M.; Yufit, D. S.; Batsanov, A. S.; Howard, J. A. K.; Marder, T. B. Crystal engineering with p-substituted 4-ethynylbenzenes using the C-H···O supramolecular synthon. *CrystEngComm* **2004**, *6*, 184–188.
- (79) Steffen, A.; Ward, R. M.; Tay, M. G.; Edkins, R. M.; Seeler, F.; van Leeuwen, M.; Palsson, L. O.; Beeby, A.; Batsanov, A. S.; Howard, J. A. K.; Marder, T. B. Regiospecific Formation and Unusual Optical Properties of 2,5-Bis(arylethynyl) rhodacyclopentadienes: A New Class of Luminescent Organometallics. *Chem. - Eur. J.* **2014**, *20*, 3652–3666.
- (80) Clegg, W.; Scott, A. J. Private Communication; CSD, 2017.
- (81) Espinoza, E. M.; Clark, J. A.; Soliman, J.; Derr, J. B.; Morales, M.; Vullev, V. I. Practical Aspects of Cyclic Voltammetry: How to Estimate Reduction Potentials When Irreversibility Prevails. *J. Electrochem. Soc.* **2019**, *166*, H3175–H3187.
- (82) Cifuentes, M. P.; Powell, C. E.; Morrall, J. P.; McDonagh, A. M.; Lucas, N. T.; Humphrey, M. G.; Samoc, M.; Houbrechts, S.; Asselberghs, I.; Clays, K.; Persoons, A.; Isoshima, T. Electrochemical, spectroelectrochemical, and molecular quadratic and cubic Nonlinear optical properties of alkynylruthenium dendrimers. *J. Am. Chem. Soc.* **2006**, *128*, 10819–10832.
- (83) Powell, C. E.; Cifuentes, M. P.; Morrall, J. P.; Stranger, R.; Humphrey, M. G.; Samoc, M.; Luther-Davies, B.; Heath, G. A. Organometallic complexes for nonlinear optics. 30. Electrochromic linear and nonlinear optical properties of alkynylbis(diphosphine) ruthenium complexes. *J. Am. Chem. Soc.* **2003**, *125*, 602–610.
- (84) Choi, S. H. C.; Frisbie, C. D., Hopping Transport in Long Conjugated Molecular Wires Connected to Metals. In *Charge and Exciton Transport through Molecular Wires*; Siebbeles, L. D. A., Grozema, F. C., Eds.; Wiley-VCH: Weinheim, Germany, 2011.
- (85) Pommerrehne, J.; Vestweber, H.; Guss, W.; Mahrt, R. F.; Bassler, H.; Porsch, M.; Daub, J. Efficient Two Layer LEDs on a Polymer Blend Basis. *Adv. Mater.* **1995**, *7*, 551–554.
- (86) Parthey, M.; Vincent, K. B.; Renz, M.; Schauer, P. A.; Yufit, D. S.; Howard, J. A. K.; Kaupp, M.; Low, P. J. A Combined Computational and Spectroelectrochemical Study of Platinum-Bridged Bis-Triarylamine Systems. *Inorg. Chem.* **2014**, *53*, 1544–1554.
- (87) Jones, S. C.; Copceanu, V.; Barlow, S.; Kinnibrugh, T.; Timofeeva, T.; Bredas, J. L.; Marder, S. R. Delocalization in platinum-alkynyl systems: A metal-bridged organic mixed-valence compound. *J. Am. Chem. Soc.* **2004**, *126*, 11782–11783.
- (88) Sakanoue, K.; Motoda, M.; Sugimoto, M.; Sakaki, S. A molecular orbital study on the hole transport property of organic amine compounds. *J. Phys. Chem. A* **1999**, *103*, 5551–5556.
- (89) Low, P. J.; Paterson, M. A. J.; Yufit, D. S.; Howard, J. A. K.; Cherryman, J. C.; Tackley, D. R.; Brook, R.; Brown, B. Towards an

understanding of structure-property relationships in hole-transport materials: The influence of molecular conformation on oxidation potential in poly(aryl) amines. *J. Mater. Chem.* **2005**, *15*, 2304–2315.

(90) Malagoli, M.; Bredas, J. L. Density functional theory study of the geometric structure and energetics of triphenylamine-based hole-transporting molecules. *Chem. Phys. Lett.* **2000**, *327*, 13–17.

(91) Low, P. J.; Bock, S. Spectroelectrochemistry: A valuable tool for the study of organometallic-alkyne, -vinylidene, -cumulene, -alkynyl and related complexes. *Electrochim. Acta* **2013**, *110*, 681–692.

(92) Gauthier, N.; Argouarch, G.; Paul, F.; Toupet, L.; Ladjarafi, A.; Costuas, K.; Halet, J. F.; Samoc, M.; Cifuentes, M. P.; Corkery, T. C.; Humphrey, M. G. Electron-Rich Iron/Ruthenium Arylalkynyl Complexes for Third-Order Nonlinear Optics: Redox-Switching between Three States. *Chem. - Eur. J.* **2011**, *17*, 5561–5577.

(93) Cui, J. S.; Wong, Y. L.; Zeller, M.; Hunter, A. D.; Xu, Z. T. Pd Uptake and H<sub>2</sub>S Sensing by an Amphoteric Metal-Organic Framework with a Soft Core and Rigid Side Arms. *Angew. Chem., Int. Ed.* **2014**, *53*, 14438–14442.

(94) Peet, W. G.; Gerlach, D. H.; Titus, D. D. Hydride complexes of iron(II) and ruthenium(II). *Inorg. Synth.* **2007**, *15*, 38–42.

(95) Fox, M. A.; Harris, J. E.; Heider, S.; Perez-Gregorio, V.; Zakrzewska, M. E.; Farmer, J. D.; Yufit, D. S.; Howard, J. A. K.; Low, P. J. A simple synthesis of *trans*-RuCl(C-CR)(dppe)<sub>2</sub> complexes and representative molecular structures. *J. Organomet. Chem.* **2009**, *694*, 2350–2358.

(96) Zalesskiy, S. S.; Ananikov, V. P.; Reay, A. J.; Fairlamb, I. J. S. Tris(dibenzylideneacetone)dipalladium(0). *Inorg. Synth.* **2018**, *37*, 183–188.

(97) Coulson, D. R.; Satek, L. C.; Grim, S. O. Tetrakis-(Triphenylphosphine)Palladium(0). *Inorg. Synth.* **2007**, *28*, 107–109.

(98) Yamaguchi, Y.; Ochi, T.; Matsubara, Y.; Yoshida, Z. Highly Emissive Whole Rainbow Fluorophores Consisting of 1,4-Bis(2-phenylethynyl)benzene Core Skeleton: Design, Synthesis, and Light-Emitting Characteristics. *J. Phys. Chem. A* **2015**, *119*, 8630–8642.

(99) Sheldrick, G. M. Crystal structure refinement with SHELXL. *Acta Crystallogr., Sect. C: Struct. Chem.* **2015**, *71*, 3–8.

(100) Parsons, S.; Flack, H. D.; Wagner, T. Use of intensity quotients and differences in absolute structure refinement. *Acta Crystallogr., Sect. B: Struct. Sci., Cryst. Eng. Mater.* **2013**, *69*, 249–259.